DEVELOPMENT OF FIBER OPTICAL DELAY LINE BASED 10 GHZ PHASE NOISE MEASUREMENT SYSTEM

A THESIS SUBMITTED TO

THE GRADUATE SCHOOL OF ENGINEERING AND SCIENCE

OF BILKENT UNIVERSITY

IN PARTIAL FULFILLMENT OF THE REQUIREMENTS FOR

THE DEGREE OF

MASTER OF SCIENCE

IN

ELECTRICAL AND ELECTRONICS ENGINEERING

By

Bilgehan Paray

February 2019

DEVELOPMENT OF FIBER OPTICAL DELAY LINE BASED 10 GHZ PHASE NOISE MEASUREMENT SYSTEM
By Bilgehan Paray
February 2019

We certify that we have read this thesis and that in our opinion it is fully adequate, in scope and in quality, as a thesis for the degree of Master of Science.

Ekmel ÖZBAY(Advisor)

Vakur Behçet Ertürk

İbrahim Tuna Özdür

Approved for the Graduate School of Engineering and Science:

Ezhan Karaşan
Director of the Graduate School

ABSTRACT

DEVELOPMENT OF FIBER OPTICAL DELAY LINE BASED 10 GHZ PHASE NOISE MEASUREMENT SYSTEM

Bilgehan Paray
M.S. in Electrical and Electronics Engineering
Advisor: Ekmel ÖZBAY
February 2019

Microwave photonics is an emerging field of study exploiting broadband, low loss photonics technology for high spectral purity microwave generation, processing and distribution. Fiber optical delay lines are such systems employed successfully for generation and phase noise analysis of microwave signals with high spectral purity. Low loss and wide bandwidth of the fiber optical delay line permits much larger delays to be realized at a reasonable loss at microwave frequencies. In this study, fiber optical delay line based frequency discriminator phase noise measurement system is designed and implemented to resolve ultra low phase noise spectra of optoelectronic oscillators. System design is described in detail including fiber optical and microwave component characterizations, selection criteria, system stabilization against environmental fluctuations and system calibration. Phase noise measurements for various RF synthesizers available in the laboratory are conducted with the developed system and compared to spectrum analyzer phase noise measurements to validate system calibration. Finally, phase noise spectra of optoelectronic oscillators (OEO) with 1 km and 2 km delay elements are demonstrated with the developed system. With 2 km OEO, system can resolve phase noise spectra as low as $-140\,\mathrm{dBc/Hz}$ at $10\,\mathrm{kHz}$ offset from $10\,\mathrm{GHz}$ carrier frequency.

Keywords: Phase noise, Frequency discriminator, Optoelectronic oscillator, Microwave photonics.

ÖZET

FİBER OPTİK GECİKME HATTI TABANLI 10 GHZ FAZ GÜRÜLTÜSÜ ÖLÇÜM SİSTEMİ GELİŞTİRİLMESİ

Bilgehan Paray
Elektrik Elektronik Mühendisliği, Yüksek Lisans
Tez Danışmanı: Ekmel ÖZBAY
Şubat 2019

Fotonik sistem elemanlarının geniş band aralığında düşük kayıplarla çalışabileme kabiliyetlerini yüksek spektral saflıkta mikrodalga sinyallerin oluşturulması, işlenmesi ve dağıtılması gibi alanlara entegre etmeyi amaçlayan mikrodalga fotoniği son yıllarda öne çıkan çalışma alanlarından biridir. Fiber optik tabanlı gecikme hatları da yüksek saflıkta mikrodalga/milimetre dalga sinyallarin oluşturulması ve faz gürültülerinin ölçülmesinde başarılı bir şekilde uygulanmış fotonik elemanlardan biridir. Düşük kayıplı ve geniş sinyal bandına sahip fiber optik gecikme hatları ile makul bir hacimde çok uzun gecikme süreleri yaratılabilmektedir. Çok yüksek spektral saflığa sahip optoeleletronik osilatör sinyal kaynaklarının faz gürültülerini ölçebilmek için, fiber optik gecikme hattı tabanlı frekans ayırıcı faz gürültülü ölçüm sistemi çalışılmıştır. Sistem tasarımı, sistem elemanlarının seçimi ve karakterizasyonu, sistemin çevresel koşullara karşı stabilizasyonu ve sistemin kalibrasyonu konuları detaylı aktarıldı. Geliştirilen sistem ile ticari RF sinyal kaynaklarının faz gürültüleri ölçüldü ve spektrum analizör ölçümleri ile karşılaştırıldı. Son olarak da 1 km ve 2 km gecikme hattına sahip optoelektronik osilatörlerin faz gürültüleri ölçüldü. Geliştirilen sistem 10 GHz taşıyıcı frekanstan 10 kHz uzaklıkta $-140\,\mathrm{dBc/Hz}$ kadar düşük faz gürültüsünü ölçebilmektedir.

Anahtar sözcükler: Faz gürültüsü, Frekans ayırıcı sistemler, optoelektronik osilatör, Mikrodalga fotoniği.

Acknowledgement

I would like to thank Dr. Tolga Kartaloğlu for his support, guidance, patience and help in my studies. His technical inputs were invaluable for the development of the system.

I would like to thank my advisor Prof. Ekmel ÖZBAY for his motivation and support.

I would like to thank Prof. Vakur Behçet Ertürk and Assoc. Prof. İbrahim Tuna Özdür for their valuable time in my thesis committee.

I am truly grateful to my friends Canberk Ünal and Faruk Uyar for their support and tolerance during laboratory studies. I would also like to thank Ayşegül Özdemir for helping me to solder electronic circuits.

Finally, I would like to thank my family for their unconditional support.

Contents

1 Introduction **1**

2 Theoretical Background **3**

2.1 Phase Noise Definition 4

2.2 Phase Noise Measurement Methods 6

2.2.1 Direct Measurement Method 7

2.2.2 Phase Locked Loop(PLL) Measurement Method 11

2.2.3 Cross Correlation Method with Two Reference Sources . . 13

2.2.4 Delay Line Frequency Discriminator Method 15

2.2.5 Delay Line Measurement System with Fiber Optical Delay Line 18

2.3 Comparison of Measurement Methods 19

3 System Design Description **21**

3.1 System Description 21

3.2 Fiber Optical Delay Line Design and Characterization 24

3.2.1 Fiber Optical Components 24

3.2.2 RF Bandwidth Characterization 37

3.2.3 Optical Power Saturation Characterization 40

3.3 Microwave Link Design and Characterization 42

3.3.1 Low Phase Noise Amplifiers 42

3.3.2 Variable Phase Shifter 43

3.3.3 Double Balanced Mixer as a Phase Detector 45

3.3.4 Quadrature Locking Circuit 47

3.4 Conclusion 50

4 System Characterization and Phase Noise Measurements of Laboratory RF Synthesizers 51

4.1 System Calibration with a known FM Tone 52

4.1.1 Calibration constant calculation 52

4.1.2 Frequency response and system linearity measurements . . 54

4.2 Phase Noise Measurements of Laboratory RF Sources 56

4.2.1 Phase Noise Floor without Delay 56

4.2.2 Phase Noise Measurement Comparisons 58

5 Conclusions 61

A Single loop optoelectronic oscillator **69**

B Matlab scripts **71**

List of Figures

2.1 The effect of amplitude and phase fluctuations in time domain . . 4

2.2 Phase noise measurement from RF power spectrum 6

2.3 Simplified block diagram of RF Spectrum Analyzer 7

2.4 Minimum Measurable Phase Noise of E4440 Spectrum Analyzer . 8

2.5 Approximation validity 10

2.6 Simplified block diagram of PLL measurement system 12

2.7 Cross correlation phase noise measurement method 14

2.8 Simplified block diagram of delay line frequency discriminator . . 16

2.9 Fiber optical delay Line with minimal components 18

2.10 Single mode fiber attenuation vs. wavelength 19

3.1 Block diagram of the measurement system 22

3.2 Laser module and relative intensity noise for 10 kHz to 40 GHz . . 25

3.3 Mach-Zehnder intensity modulator with single-arm drive 25

3.4 Nonlinear response of Mach-Zehnder modulator 27

3.5 Modulator drive power budget 28

3.6 Two-tone V_π measurement system 29

3.7 Half wave voltage measurement for modulator one 33

3.8 Comparing theoretical sideband to carrier ratio to measured values for modulator one. 33

3.9 Half wave voltage measurement for modulator two 34

3.10 Comparing theoretical sideband to carrier ratio to measured values for modulator two. 34

3.11 Core, cladding and coating of the single mode optical fiber 35

3.12 OTDR measurement of the optical fiber 36

3.13 RF bandwidth of photodetector 37

3.14 RF bandwidth measurement of the delay line 37

3.15 RF bandwidth measurement with 5 km single mode fiber delay . . 39

3.16 RF bandwidth measurement with 20 km near zero dispersion shifted fiber delay 39

3.17 SBS threshold power measurement setup for fiber optical fiber . . 40

3.18 SBS threshold measurement for 5 km SMF 41

3.19 SBS threshold measurement for 20 km SMF 41

3.20 Residual phase noise of LPN1 and LPN3 at $P_{out} = 10\,\mathrm{dBm}$ 43

3.21 Residual phase noise of LPN1 and LPN3 at $P_{out} = 10\,\mathrm{dBm}$ at $9\,\mathrm{GHz}$ 43

3.22 Phase shift vs. control voltage 44

3.23 Control voltage vs. insertion loss 45

3.24 Mixer saturation power measurement setup 46

3.25 Mixer saturation power measurement 46

3.26 Schematics of quadrature locking circuit 48

3.27 Quadrature locking circuit first stage 49

3.28 Quadrature locking circuit second stage 49

4.1 Calibration FM signal generation 52

4.2 Calibration FM signal power spectrum. 53

4.3 Demodulated output voltage when calibration FM is injected to system. 53

4.4 Baseband frequency response of the system 55

4.5 Linearity of the system 55

4.6 Frequency domain noise floor of the system with zero delay. . . . 57

4.7 Time domain trace of system noise floor with zero delay. 57

4.8 Phase noise measurement of Hittite T2100 RF synthesizer. 58

4.9 Phase noise measurement of HP 83620B RF synthesizer. 59

4.10 Phase noise measurement of OEO with 1 km delay. 59

4.11 Phase noise measurement of OEO with 2 km delay. 60

A.1 Block diagram of optoelectronic oscillator. 70

List of Tables

3.1 Laser parameters. 24

3.2 Power measurements for modulator one 32

3.3 Power measurements for modulator two 32

3.4 Specifications of the optical fiber 35

3.5 Photodetector specifications. 37

3.6 Specifications for LPN1 and LPN3. 42

3.7 Specifications for LPN2 and LPN4. 42

3.8 Specifications for electronically controlled phase shifter. 44

3.9 Specifications for the double balanced mixer. 45

Chapter 1

Introduction

Microwave photonics has gained remarkable attraction in generation and processing of microwave and millimeter wave signals[1][2]. Wide bandwidth and low loss advantages of microwave photonics components have found many applications in microwave/millimeter wave systems such as phased array antenna beam forming[3], wideband tunable microwave filters[4], analog-to-digital converters[5], arbitrary waveform generation[6], high spectral purity microwave/millimeter wave signal generation[7] and phase noise measurement of microwave signals[8].

Microwave photonics delay lines are also such systems offering very long time delays realizable with reasonable loss[9]. Possibility of such long delays in compact volumes paved the way for systems such as optoelectronic oscillators and delay line discriminators where the longer delays are critical in achieving better system performance. Initial analyses for integration of optical delays into the microwave systems goes back to early 90s[10]. The ideas in reference [10] are first applied by a team of engineers in NASA Jet Propulsion Laboratory to generate microwave/millimeter wave signals with very high spectral purity[7]. The same group, in reference [11], demonstrated high spectral purity microwave signal with phase noise of $-165\,\mathrm{dBc/Hz}$ at around $10\,\mathrm{kHz}$ offset from $10\,\mathrm{GHz}$ center frequency, which was the lowest phase noise for microwave signals demonstrated at that date.

Practical ease in creating such signals with high spectral purity constituted a necessity for systems capable to resolve ultra low close-in phase noise of these signals. The integration of fiber optical delay into well-known delay line frequency discriminator phase noise measurement method offered an exceptional solution to this problem[8]. In reference [12], cross correlation microwave phase noise measurement system with a phase noise floor of $-165\,\mathrm{dBc/Hz}$ at $10\,\mathrm{kHz}$ offset from $10\,\mathrm{GHz}$ carrier frequency is demonstrated with 500 averages and with a $2\,\mathrm{km}$ dual delay line frequency discriminator system.

The thesis begins with a survey of phase noise measurement methods and compares different methods for the suitability for phase noise measurement of optoelectronic oscillators. With the advantage of long delay, frequency discriminator technique appears to be the best method for this purpose. Next, system design is described including component characterizations, selection criteria, stabilization circuit for environmental fluctuations. Then, system calibration, linearity, frequency response and noise floor characterization measurements are discussed in the last section. Phase noise measurements of laboratory synthesizers and optoelectronic oscillators are conducted with the developed system and compared to spectrum analyzer measurements. Developed system can successfully resolve phase noise as low as $-140\,\mathrm{dBc/Hz}$ at $10\,\mathrm{kHz}$ offset from $10\,\mathrm{GHz}$ carrier frequency without any cross correlation.

Chapter 2

Theoretical Background

The instantaneous voltage of a noise-free ideal oscillator can be represented with a pure sinusoidal function

$$v(t) = V_0 \sin(2\pi \upsilon_0 t + \Phi_0) \tag{2.1}$$

where V_0 denoting the nominal amplitude, υ_0 the nominal frequency and Φ_0 the constant phase shift. However, to account for fluctuations in amplitude and frequency, instantaneous voltage of a real world oscillator is modeled with the quasi-perfect sinusoidal function[13]

$$v(t) = [V_0 + \epsilon(t)] \sin(2\pi \upsilon_0 t + \Phi(t)) \tag{2.2}$$

where $\epsilon(t)$ denotes fluctuation in nominal amplitude, $\Phi(t)$ fluctuation in nominal phase. The effect of amplitude and phase fluctuations on ideal sinusoidal signal is illustrated in Figure 2.1a and 2.1b respectively[14]. From Figure 2.1a, fluctuations in amplitude does not alter periodic zero crossing locations. Whereas, from Figure 2.1b, zero crossings of quasi-sinusoidal signal under the influence of phase fluctuations deviate from periodic crossings because fluctuations in phase results in fluctuations in frequency as [13]

$$y(t) \equiv \frac{\upsilon(t) - \upsilon_0}{\upsilon_0} = \frac{\dot{\Phi}(t)}{2\pi \upsilon_0} \tag{2.3}$$

where $y(t)$ is the normalized frequency fluctuations.

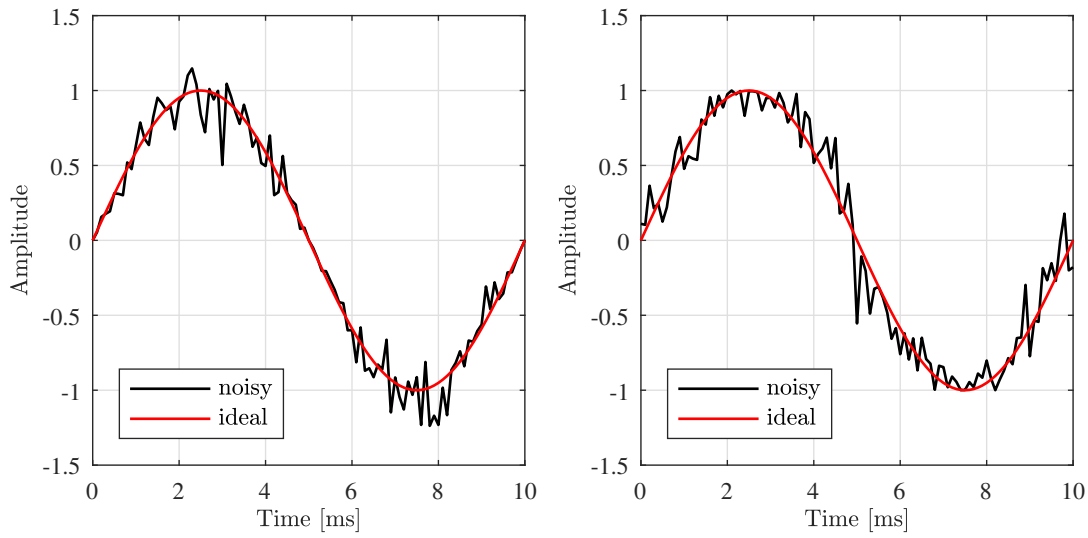

(a) Amplitude fluctuations (b) Phase fluctuations

Figure 2.1: The effect of amplitude and phase fluctuations in time domain

2.1 Phase Noise Definition

Phase fluctuations $\Phi(t)$ in equation 2.2 can take four different forms three of which can be depicted mathematically as follows[15]

$$\Phi(t) = D_1 t^2 + \Delta\Phi \sin(2\pi f_m t) + \phi(t) \tag{2.4}$$

The first term, $D_1 t^2$, in equation 2.4 represents long term drifts from the nominal frequency υ_0. On the ground that frequency and phase fluctuations are related through the equation 2.3, then

$$y(t) = \frac{2D_1 t}{2\pi \upsilon_0} \tag{2.5}$$

where D_1 is the drift constant in s^{-2}. For example, aging rate of Hittite T2100 synthesized signal generator is specified as 1 ppm/yr[16]. Assuming $\upsilon_0 = 10\,\text{GHz}$, D_1 can be calculated as

$$y(t) = \frac{2D_1 \times 31556926}{2\pi 10 \times 10^9} = \frac{1}{10^6} \rightarrow D_1 = 9.95532\text{e-}4\ [s^{-2}] \tag{2.6}$$

where $t = 31\,556\,926$ seconds in one year. Hence, D_1 characterizes deterministic, long term fluctuations and its effect is negligible unless time scale is on the order

of years. Long term fluctuations are not characterized by the system described in this thesis and neglected in the rest of the study.

The second term, $\Delta\Phi \sin(2\pi f_m t)$, in equation 2.2 embodies periodic perturbations in phase. Periodic perturbations might be due to interference from a noisy power supply or can represent a known FM message signal[15].

The last term, $\phi(t)$, in equation 2.2 illustrates short term, random phase fluctuations and also termed as the phase noise of the oscillator. The system under study provides frequency domain measurement of phase noise $\phi(t)$.

The fourth perturbation not modeled mathematically is the abrupt changes in nominal frequency, also called frequency hopping[15].

Neglecting long term drifts and frequency hopping effects, $D_1 t^2$ and periodic phase fluctuations, $\Delta\Phi \sin(2\pi f_m t)$, the instantaneous voltage of a noisy oscillator reduces to

$$v(t) = [V_0 + \epsilon(t)] \sin(2\pi \upsilon_0 t + \phi(t)) \tag{2.7}$$

Oscillator phase noise is defined as the half of the one sided power spectral density of random phase fluctuations $\phi(t)$[17]

$$S_\phi(f) = \mathbf{E}\{\mathcal{F}\{R_\phi(t_1, t_2)\}\} \left[\frac{rad^2}{Hz}\right] \tag{2.8}$$

$$\mathcal{L}(f) = \frac{S_\phi(f)}{2} \left[\frac{dBc}{Hz}\right] \tag{2.9}$$

where R_ϕ is the autocorrelation function of $\phi(t)$. Following the Wiener-Khinchin theorem, S_ϕ is the expected value of Fourier Transform of the autocorrelation function. $\mathcal{L}(f)$ is the main parameter of interest when characterizing phase noise where frequency f denotes the frequency offset from the carrier. Since only a finite number of samples are available for $\phi(t)$, S_ϕ can be estimated using periodogram with the assumption that $\phi(t)$ is an ergodic process[17]

$$S_\phi(f) = |\mathcal{F}\{\phi(t)\}|^2 \tag{2.10}$$

For all phase noise calculations, MATLAB's periodogram function with rectangular window is invoked. Specified number of periodograms are averaged to smooth periodogram estimates.

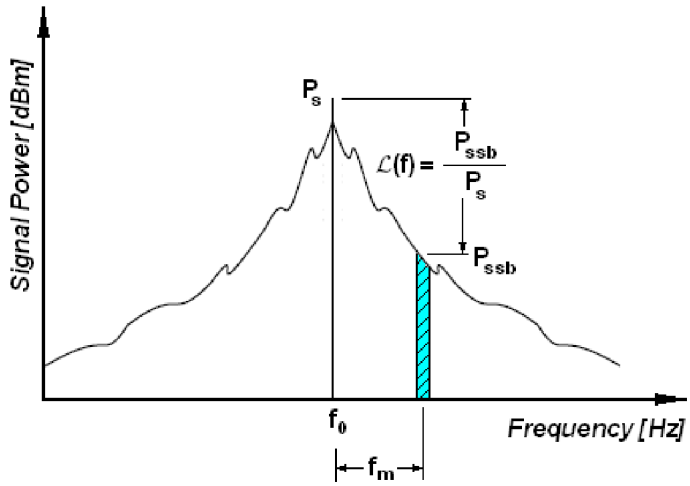

Figure 2.2: Phase noise measurement from RF power spectrum, adapted from [18]

However obsolete, $\mathcal{L}_f$ has another definition relating spectral power density at noise sidebands to phase noise spectrum as [13]

$$\mathcal{L}(f) = \frac{\text{power density in one phase noise modulation sideband}}{\text{total signal power}} \left[\frac{dBc}{Hz}\right] \quad (2.11)$$

The inherent difference between the definition in equation 2.10 and 2.11 is that the spectrum in equation 2.11 is usually obtained with a spectrum analyzer. However, to obtain the phase noise spectrum in equation 2.9, RF signal is demodulated into baseband by an appropriate frequency or phase demodulator. Limitations for spectrum analyzer phase noise measurements and conditions for validity of the measurements are discussed in subsequent sections. Figure 2.2 summarizes the procedure to obtain phase noise spectrum from RF power spectrum.

2.2 Phase Noise Measurement Methods

Time domain phase noise measurement of microwave sources above 1 GHz is an arduous task because of difficulty in obtaining period counter devices operating at this frequency range[19]. Thus, frequency domain phase noise measurement techniques of high frequency microwave sources are reviewed in this section.

2.2.1 Direct Measurement Method

Direct measurement of phase noise spectrum of a noisy oscillator is through the definition given in equation 2.11. A simplified block diagram of a superheterodyne RF spectrum analyzer is highlighted in Figure 2.3 to identify the limitations of the measurement system[20].

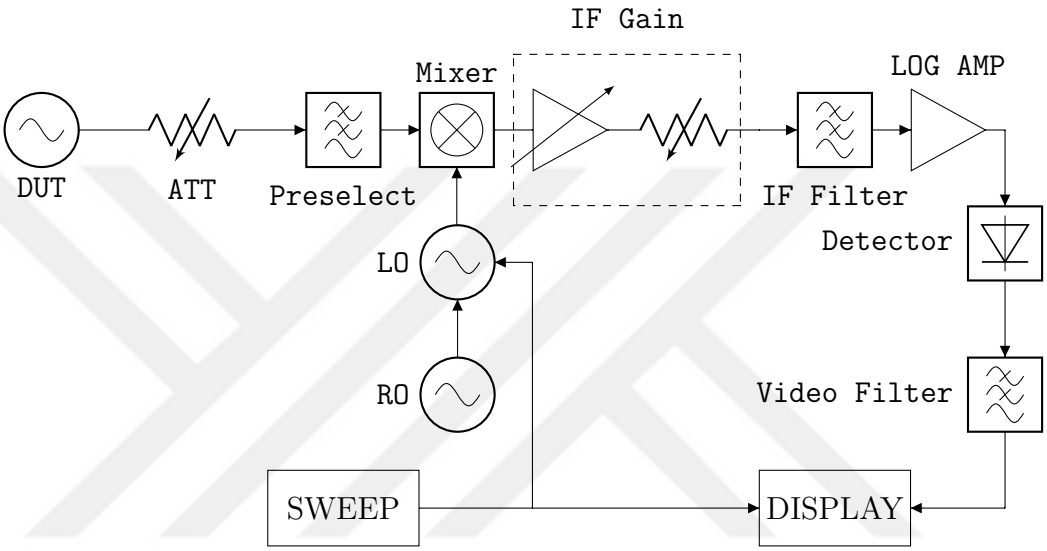

Figure 2.3: Simplified block diagram of RF Spectrum Analyzer[20]. DUT: Device Under Test, ATT: Input Attenuator, Preselect: Input Preselector, LOG AMP: Logarithmic Amplifier, LO: Local Oscillator, RO: Reference Oscillator.

From Figure 2.3, the RF input is first downconverted with a local oscillator whose frequency is swept over the measurement bandwidth. The phase noise of the local oscillator has detrimental effect on the minimum measurable phase noise of the device under test. Neglecting amplitude fluctuations, intermediate frequency (IF) output of the mixer can be simply obtained as

$$v(t) = V_0 \sin(2\pi \upsilon_0 t + \phi(t)) \tag{2.12}$$

$$\upsilon_{LO} = V_{LO} \sin(2\pi \upsilon_{LO} t + \phi_{LO}(t)) \tag{2.13}$$

$$\upsilon_{IF} = V_{IF} \sin(2\pi \upsilon_{IF} t + \phi(t) - \phi_{LO}(t)) \tag{2.14}$$

where V_0, V_{LO}, V_{IF} being the input, LO and IF amplitudes, υ_0, υ_{LO}, $\upsilon_{IF} = \upsilon_0 - \upsilon_{LO}$ denoting the input, LO and IF frequencies and $\phi(t), \phi_{LO}(t)$ are the phase fluctuations of input and LO signal. From equation 2.14, phase noise of the IF signal

includes contributions from both input signal and LO signal. Hence, phase noise of the oscillator under test must be sufficiently higher than that of the local oscillator for proper measurement. The effect is exacerbated if there are multiple down conversion stages where phase noise from each LO will further degrade sensitivity[21]. Minimum measureable phase noise values at various center frequencies are plotted in Figure 2.4 for E4440 spectrum analyzer, which is the spectrum analyzer available at the laboratory.

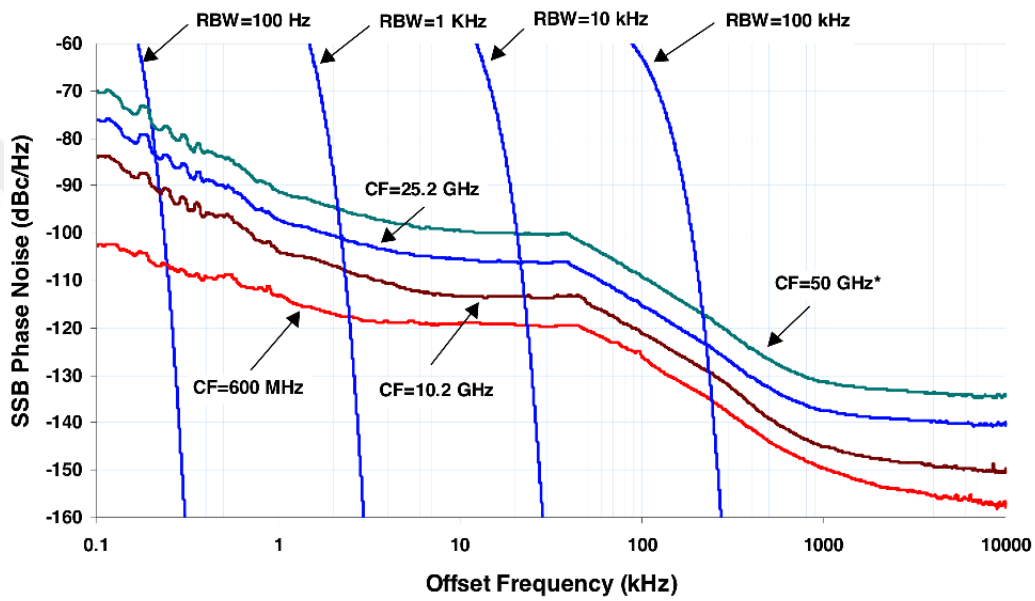

Figure 2.4: Minimum Measurable Phase Noise of E4440 Spectrum Analyzer[22]

Another remarkable shortcoming of the measurement method is the limited resolution bandwidth of the spectrum analyzer. After IF gain adjustment, 3 dB bandwidth of the IF filter sets the desired resolution bandwidth of the measurement. Hence, for example, to obtain a phase noise spectrum with a spectral resolution of 0.1 Hz, spectrum analyzer must have an IF filter with a very narrow 3 dB bandwidth, which would be impractical to realize. Minimum achievable resolution bandwidth of the available Agilent E4440A Spectrum Analyzer is 1 Hz.

Finally, because spectrum analyzer is indirectly measuring the phase noise spectrum from the power spectrum, linearity of the measurement is of concern for high phase fluctuations[23]. Following subsections investigate this limitation and outline the region of validity for the phase noise measurements.

2.2.1.1 Power Spectrum of a Sinusoidal with Periodic Phase Fluctuations

Starting with a simple case, assume amplitude fluctuations are negligible and phase fluctuations are periodic. Hence

$$\phi(t) = \Delta\Phi \cos(\omega_a t) \tag{2.15}$$

$$v(t) = V_0 \sin(2\pi \upsilon_0 t + \Delta\Phi \cos(\omega_a t)) \tag{2.16}$$

Where ω_a the denotes modulating frequency and $\Delta\Phi$ the modulation index. Using phasor notation, equation 2.16 can be rewritten as

$$v(t) = \Re\{V_0 \exp(j\pi/2) \exp(j2\pi\upsilon_0 t) \exp(\Delta\Phi \cos(\omega_a t))\} \tag{2.17}$$

Using the Jacobi-Anger expansion given in equation 2.18[24],

$$\exp(ja\cos\theta) = \sum_{m=-\infty}^{\infty} j^m J_m(a) \exp(jm\theta) \tag{2.18}$$

$$v(t) = \Re\{V_0 \exp(j\pi/2) \exp(j2\pi\upsilon_0 t) \sum_{m=-\infty}^{\infty} j^m J_m(\Delta\Phi) \exp(jm\omega_a t)\} \tag{2.19}$$

J_m in equation 2.18 and 2.19 is the Bessel function of the first kind with order being m. From equation 2.19 one can see that phase modulated RF has many frequency components at harmonics of modulation frequency. In order to invoke the definition of $\mathcal{L}(f)$ in equation 2.11, one has to identify carrier and sideband amplitudes. For $m = 0$, carrier amplitude is proportional to $J_0(\Delta\Phi)$, for $m = 1$ sideband amplitude is proportional to $J_1(\Delta\Phi)$ and other sideband amplitudes are similarly proportional to higher order Bessel functions. To invoke small argument assumption, asymptotic approximation of Bessel functions are given as[25]

$$J_m(z) \approx \frac{1}{\Gamma(m+1)} \left(\frac{z}{2}\right)^m \tag{2.20}$$

$$J_0(z) \approx 1 \tag{2.21}$$

$$J_1(z) \approx \frac{z}{2} \tag{2.22}$$

$$J_m(z) \approx 0 \text{ for higher order terms.} \tag{2.23}$$

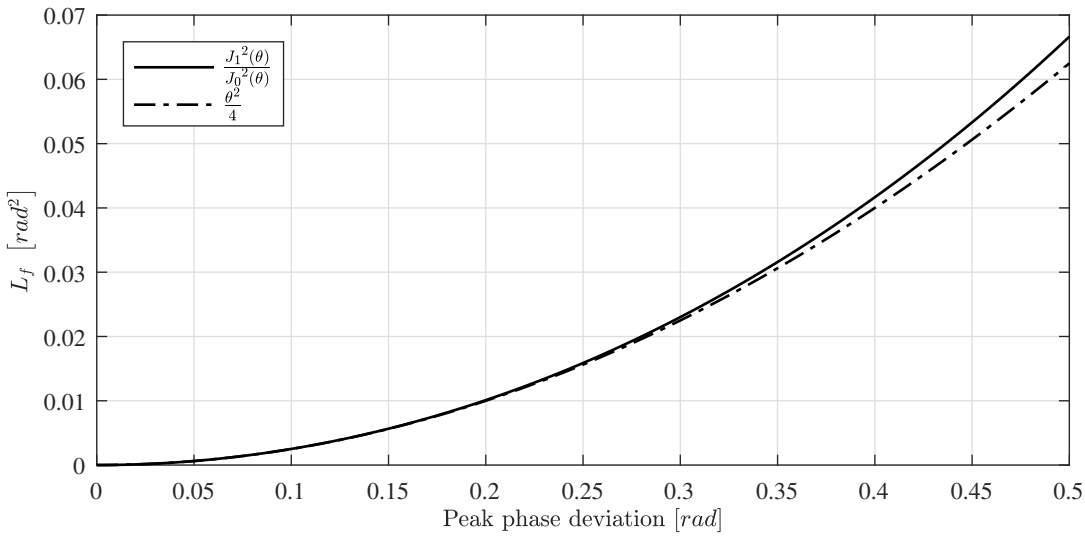

Figure 2.5: Approximation validity

Hence invoking equation 2.11

$$\mathcal{L}(f) = \frac{\left(\frac{\Delta\Phi}{2}\right)^2 / \ 2}{1/2} = \frac{(\Delta\Phi)^2}{4} \tag{2.24}$$

Power spectrum of phase fluctuations would also be obtained by using 2.10 directly as

$$S_\phi(f) = \frac{(\Delta\Phi)^2}{2} \tag{2.25}$$

Therefore, phase noise measurements from a spectrum analyzer is valid only if phase fluctuations are small so that one can approximate Bessel functions with its asymptotic values. Figure 2.5 highlights the deviation of asymptotic approximation from actual value. As a rule of thumb, peak phase deviations smaller than 0.2 radians are considered to be small and deviation from actual value is about %0.1[23].

2.2.1.2 Power Spectrum of a Sinusoidal with Random Phase Fluctuations

When the phase fluctuation is assumed to be a stationary Gaussian random process and amplitude fluctuations neglected, RF power spectrum is related to

phase noise spectrum through[15]

$$S_v(f) = \frac{{V_0}^2}{2} \exp\left(-\langle\phi^2\rangle\right) \{\delta(f - \upsilon_o) + {S_\phi}^{TS}(f - \upsilon_0) + \sum_{n=2}^{\infty} \frac{1}{n!} \left[{S_\phi}^{TS}(f) \overset{n-1}{\circledast} {S_\phi}^{TS}(f)\right]_{\upsilon_0} \} \tag{2.26}$$

Where $\langle\phi^2\rangle$ denoting the mean square of $\phi(t)$, ${S_\phi}^{TS}(f)$ two-sided power spectral density of $\phi(t)$ and the infinite summation term represents $n-1$ convolutions of the power spectral density

$$\left[{S_\phi}^{TS}(f) \overset{n-1}{\circledast} {S_\phi}^{TS}(f)\right]_{\upsilon_0} = \left[\underbrace{{S_\phi}^{TS}(f) \circledast {S_\phi}^{TS}(f) \circledast {S_\phi}^{TS}(f) \cdots}_{n-1}\right]_{\upsilon_0} \tag{2.27}$$

The subscript υ_0 signifies the up-conversion of the spectrum to the carrier frequency υ_0. Equation 2.26 is also known as Middleton's convolution series and reduces to following for low phase noise case $\langle\phi^2\rangle \ll 1$ [26]

$$S_v(f) = \frac{{V_0}^2}{2}\{\delta(f - \upsilon_o) + {S_\phi}^{TS}(f - \upsilon_0)\} \tag{2.28}$$

The ideal oscillator spectrum would only consists of a delta function at the carrier frequency. Phase noise measurement can be readily obtained by invoking the definition given in Figure 2.2. Similar to periodic modulation case, the measurement is increasingly invalid for higher phase noise due to contributions from the convolution terms.

2.2.2 Phase Locked Loop(PLL) Measurement Method

Phase and frequency demodulation techniques are developed to circumvent shortcomings of direct power spectrum measurements[15]. Heterodyning the oscillator under test with a stable reference oscillator whose frequency is locked to the oscillator with a phase locked loop (PLL) is one of the widely employed phase demodulation scheme to measure phase noise spectra[27]. Figure 2.6 shows the simplified block diagram of the measurement system.

In Figure 2.6, Φ_0, $\dot{\Phi}_0$ denotes Laplace transform of phase and frequency fluctuations of oscillator under test respectively, Φ_r, $\dot{\Phi}_r$ of reference oscillator, $H_1(s)$ is

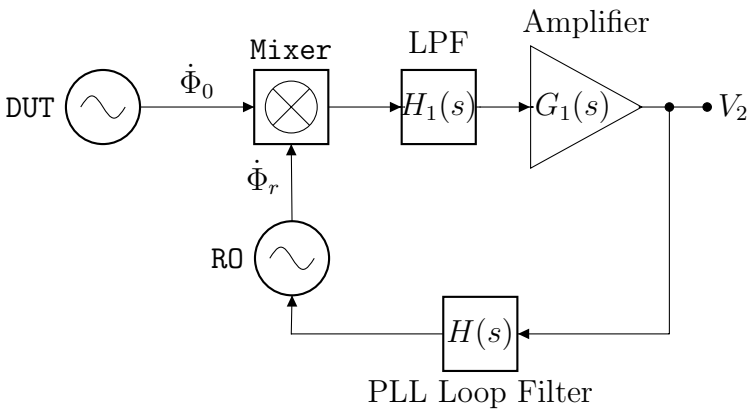

Figure 2.6: Simplified block diagram of PLL measurement system[28]. DUT: Device Under Test, RO: Reference Oscillator, LPF: Low Pass Filter, V_2 Output Voltage

the low pass filter to remove $2f$ component, $G_1(s)$ is the amplifier and finally $H(s)$ is the PLL loop filter. Assuming the phase detector is operating within its linear range with a sensitivity of μ with units of Volts per radians, a phase-to-voltage Laplace transfer function can be calculated as[28]

$$V_2 = \frac{\mu G_1(s)}{1 + (\mu/s)\, K G_1(s) H(s)} \left[\Phi_0 - \Phi_r\right] \tag{2.29}$$

where K is sensitivity of the reference oscillator frequency control with units of radians per second per volt. Several conclusions can be drawn from equation 2.29 to analyze technique's limitations.

To begin with, output voltage is proportional to $[\Phi_0 - \Phi_r]$ which also contains phase fluctuations from the reference source. Assume that phase fluctuations of reference oscillator $\phi_r(t)$ and oscillator under test $\phi_0(t)$ are uncorrelated wide sense stationary random processes, we can calculate the auto-correlation function of the difference as[28]

$$\phi(t) = \phi_0(t) - \phi_r(t) \tag{2.30}$$

$$R(\tau) = \mathbf{E}\{\phi(t+\tau)\phi(t)\} \tag{2.31}$$

$$= \mathbf{E}\{(\phi_0(t+\tau) - \phi_r(t+\tau))\,(\phi_0(t) - \phi_r(t))\} \tag{2.32}$$

$$= \mathbf{E}\{\phi_0(t+\tau)\phi_0(t)\} + \mathbf{E}\{\phi_r(t+\tau)\phi_r(t)\} \tag{2.33}$$

Cross terms in 2.33 are zero due to uncorrelation assumption. Then we have

$$R(\tau) = R_0(\tau) + R_r(\tau) \tag{2.34}$$

From the Wiener Khincinite theorem, power spectral density of the difference is the sum of the two

$$S(f) = S_0(f) + S_r(f) \tag{2.35}$$

Hence from equation 2.35, to measure the spectral density of the phase noise of oscillator under test, a reference oscillator with a much lower phase noise must be used. In order to measure $-140\,\mathrm{dBc/Hz}$ phase noise at $10\,\mathrm{kHz}$ offset at $10\,\mathrm{GHz}$ center frequency requires a state of the art reference oscillator with a phase noise of at least $-150\,\mathrm{dBc/Hz}$ phase noise at $10\,\mathrm{kHz}$ at the same frequency. This stringent requirement on the reference source is the main driving reason to disregard PLL measurement method over the delay line method described in this thesis.

Furthermore, frequency response in equation 2.29 has high pass characteristics since both $G_1(s)$ and $H(s)$ are designed to have low pass characteristics. The sensitivity of the system degrades below the cut-off frequency of the transfer function.

2.2.3 Cross Correlation Method with Two Reference Sources

Cross correlation measurement method is in principle based on the fact that uncorrelated signals add up incoherently whereas correlated signals add up coherently. Hence, if the phase noise of oscillator under test is measured with two different systems whose background noise including contributions from the reference sources are uncorrelated, it may be possible to measure the phase noise of a source with another reference source whose phase noise is higher than the source under test[29]. Figure 2.7 shows the simplified block diagram of the measurement system.

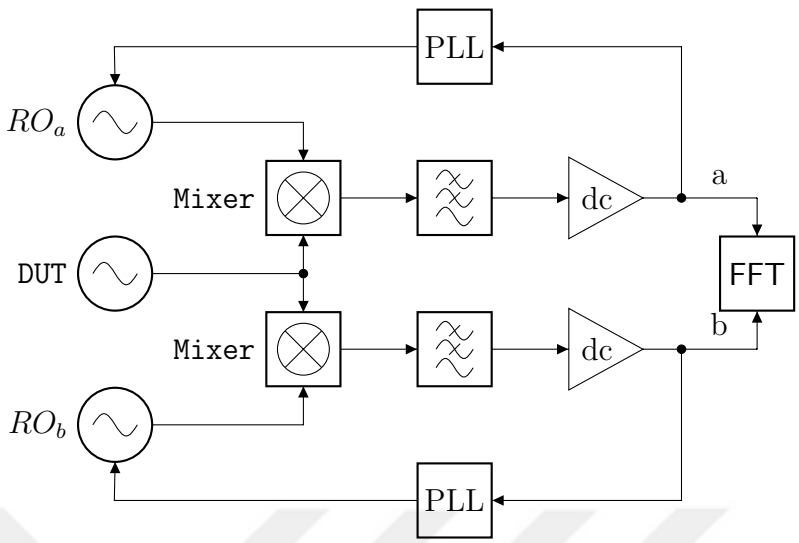

Figure 2.7: Cross Correlation Phase Noise Measurement Method[29]. RO_a: Reference oscillator a, RO_b Reference oscillator b, DUT: Device under test, FFT: Fast Fourier Transform analyzer

From Figure 2.7 and equation 2.29, let the time domain signal in two separate arms be

$$\phi_{2a} = (\phi_0(t) - \phi_{ra}(t)) \tag{2.36}$$

$$\phi_{2b} = (\phi_0(t) - \phi_{rb}(t)) \tag{2.37}$$

Where ϕ_0, ϕ_{ra}, ϕ_{rb} are ergodic, stationary and independent random processes representing phase fluctuations of oscillator under test, reference source a and reference source b, respectively. To find the cross spectrum, cross correlation of the signals in two different arms are calculated

$$R_{ab}(t, t+\tau) = \mathbf{E}\{\phi_{2a}(t)\phi_{2b}(t+\tau)\} \tag{2.38}$$

$$= \mathbf{E}\{[\phi_0(t) - \phi_{r1}(t)]\,[\phi_0(t+\tau) - \phi_{r2}(t+\tau)]\} \tag{2.39}$$

$$= \mathbf{E}\{\phi_0(t)\phi_0(t+\tau)\} - \mathbf{E}\{\phi_0(t)\phi_{r2}(t+\tau)\} -$$

$$\mathbf{E}\{\phi_{r1}(t)\phi_0(t+\tau)\} + \mathbf{E}\{\phi_{r1}(t)\phi_{r2}(t+\tau)\} \tag{2.40}$$

Invoking the independence assumption to the 2.40, we find that cross spectrum converges to auto-correlation of the source phase noise[29].

$$R_{ab}(t, t+\tau) = \mathbf{E}\{\phi_0(t)\phi_0(t+\tau)\} \tag{2.41}$$

Notice that in practice, because number of samples of a random process is finite, sample averages are calculated instead of the expectation. The uncorrelated terms converge to zero with increasing number of averages with the order of $1/\sqrt{m}$[29].

Hence, to reject 20 dB of instrument noise, one has to average 10 000 measurements. Assuming each measurement takes 1 s to complete, total measurement time is increased to nearly 3 h. The measurement time is traded off for increased background noise rejection. Furthermore, two channel measurement system with distinct parts are required to maintain inter-channel independence of the background noise. Therefore, number of components and the total cost are doubled with respect to single reference source PLL measurement system.

For example, in order to measure an ultra low phase noise of −140 dBc/Hz at 10 kHz offset at 10 GHz center frequency, assuming 10 000 cross-correlation averages, two reference sources with phase noise better than −120 dBc/Hz at same frequency are required. The RF synthesizers Hittite T2100 and HP83620B have inherent phase noise much higher than this value[16][30]. Thus, because necessity of low phase noise reference source is not quite removed, cross correlation measurement system is also a disregarded candidate solution.

2.2.4 Delay Line Frequency Discriminator Method

Delay line frequency discriminator method is based on frequency demodulation of the oscillator signal under test without utilizing another reference source. The system achieves this by mixing the carrier with a delayed replica of itself using a delay stage and a double balanced mixer operating as a phase detector[23]. Simplified block diagram is provided in Figure 2.8.

Transfer function of the system can be easily obtained in time domain assuming

the oscillator under test has the form in equation 2.42

$$v(t) = V_0 \sin(2\pi \upsilon_0 t + \phi(t)) \tag{2.42}$$

$$v_{LO}(t) = V_0 \sin(2\pi \upsilon_0 (t+\tau) + \phi(t+\tau)) \tag{2.43}$$

$$v_{RF}(t) = V_0 \sin(2\pi \upsilon_0 (t) + \phi(t) + \Phi) \tag{2.44}$$

where v_{RF} and v_{LO} represents voltages at RF and LO arms of the mixer, $v(t)$ is the oscillator signal under test, Φ denotes the constant phase offset incurred by variable phase shifter to maintain quadrature condition at the RF and LO arms. After mixing the terms and low pass filtering the 2ω term, DC term is obtained

$$v_0(t) = k_\phi \left(\frac{{V_0}^2}{2}\right) \cos\left(2\pi \upsilon_0 \tau + \phi(t+\tau) - \phi(t) + \Phi\right) \tag{2.45}$$

In equation 2.45, the term $2\pi \upsilon_0 \tau$ is the phase offset for the measurement and can fluctuate depending on frequency and/or delay fluctuations. In order to mitigate drift errors associated with this phase offset, Φ is adjusted such that the sum $2\pi \upsilon_0 \tau + \Phi = 90°$ and quadrature condition is maintained. In Figure 2.8 double balanced mixer operating as a phase detector is assumed to be operating in linear region with a phase-to-voltage constant k_ϕ in Volts/radians[31].

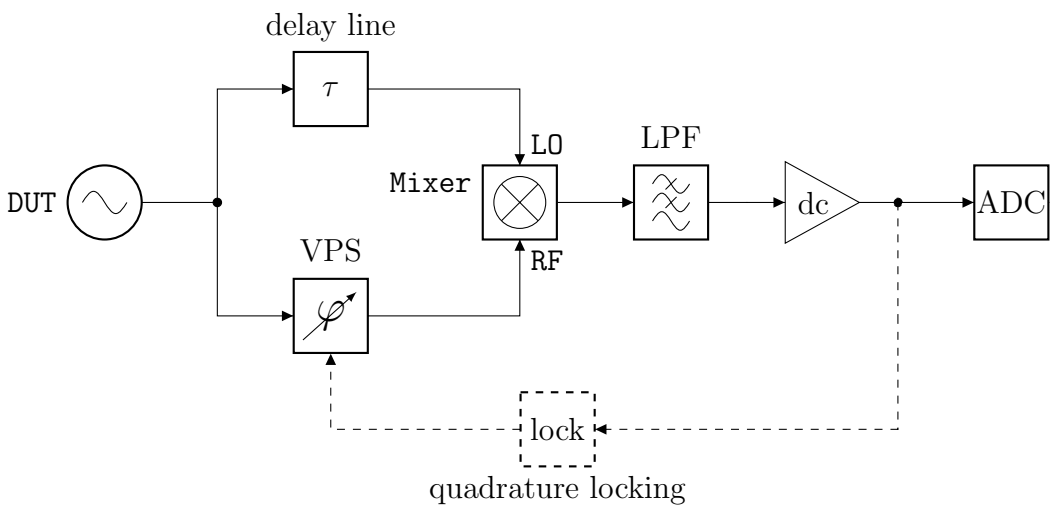

Figure 2.8: Simplified block diagram of delay line frequency discriminator[32]. DUT: Device Under Test, VPS: Variable Phase Shifter, LPF: Low Pass Filter, ADC: Analog to Digital Converter, LO: Local Oscillator Port of the Mixer, RF: Radio Frequency port of the Mixer

Then the output voltage is simplified to

$$v_0(t) = k_\phi \left(\frac{{V_0}^2}{2}\right) [\phi(t+\tau) - \phi(t)] \tag{2.46}$$

Since 2.46 is linear, Fourier transform can be applied to obtain the transfer function[8]

$$V_0(j\omega) = k_d \Phi(j\omega) [1 - \exp(-j\omega\tau)] \tag{2.47}$$

$$H_\phi(j\omega) = k_d [1 - \exp(-j\omega\tau)] \tag{2.48}$$

$$|H_\phi(j\omega)|^2 = 4{k_d}^2 \sin^2(\pi f \tau) \tag{2.49}$$

$$|H_y(j\omega)|^2 = 4{k_d}^2 \frac{{\upsilon_0}^2}{f^2} \sin^2(\pi f \tau) \tag{2.50}$$

where $V_0(j\omega)$ and $\Phi(j\omega)$ are the Fourier transforms of voltage $v_0(t)$ and phase $\phi(t)$. $H_\phi(j\omega)$ and $H_y(j\omega)$ are voltage to phase and frequency transfer functions of the measurement system. Note that equation 2.3 is employed to compute transfer function for frequency fluctuations given in equation 2.50. Several remarks can be underlined for equation 2.49. First of all, notice that f refers to slow-time scale i.e. frequency offset from the carrier. Also, k_d is the end-to-end system measurement constant including mixer phase-to-voltage conversion factor. The measurement transfer function has multiple nulls at frequency offsets corresponding to

$$\pi f \tau = n\pi, n = 0, 1, ... \tag{2.51}$$

$$f = \frac{n}{\tau} \tag{2.52}$$

Above the first null at $f = 1/\tau$ the measurement is not possible[8]; therefore the measurement bandwidth of the system is limited to frequencies much smaller than the first offset i.e. $\pi f \tau << 1$. Transfer functions given in equations 2.49 and 2.50 can be rewritten using this approximation

$$|H_\phi(j\omega)|^2 = 4{k_d}^2 \pi^2 f^2 \tau^2 \tag{2.53}$$

$$|H_y(j\omega)|^2 = 4{k_d}^2 \pi^2 {\upsilon_0}^2 \tau^2 \tag{2.54}$$

Hence from equations 2.53 and 2.54, the sensitivity of the system increases linearly with the inserted delay. However, increased sensitivity is traded-off against the reduced measurement bandwidth.

At the quadrature condition, mixer output is stabilized to zero volts[31]. Acknowledging this fact, *lock* block diagram in Figure 2.8 is designed to be an operational amplifier(OPAMP) based analog integrator circuit resulting in zero error at the output. The details of the quadrature locking circuit is elucidated in the subsequent chapter.

2.2.5 Delay Line Measurement System with Fiber Optical Delay Line

Traditional delay line frequency discriminators utilized coaxial RF cables to create sufficient delay to increase sensitivity[23]. However, RF coaxial cables come with a devastating 2dB/meter loss penalty and bulky with accommodating large space and bearing large mass. In recent studies[8][32], fiber optical delay line based on inexpensive, low loss single mode fiber is found to be very suitable to implement very long delays with reasonable loss and compact size. For example, 5 km fiber winding with a diameter of just 15 cm is easily available to create a 25 µs delay with an attenuation of only 1 dB.

A typical fiber optical delay line with minimal components is illustrated in Figure 2.9.

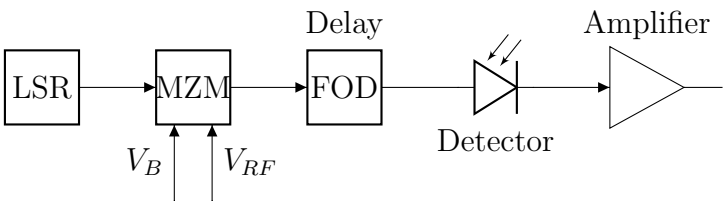

Figure 2.9: Fiber optical delay Line with minimal components [33]. LSR: Laser, MZM: Mach-Zehnder Modulator, FOD: Fiber Optical Delay, V_B: DC bias of and V_{RF}: RF input the optical modulator

The fiber optical delay line consists of a laser as the optical source, Mach-Zehnder electro-optical intensity modulator for electro-optical conversion and a fast photodetector for opto-electrical conversion. Amplifier compensates loss incurred by electro-optical and opto-electrical conversion losses. The fiber cable is

single mode fiber[34] with an attenuation against wavelength is plotted in Figure 2.10.

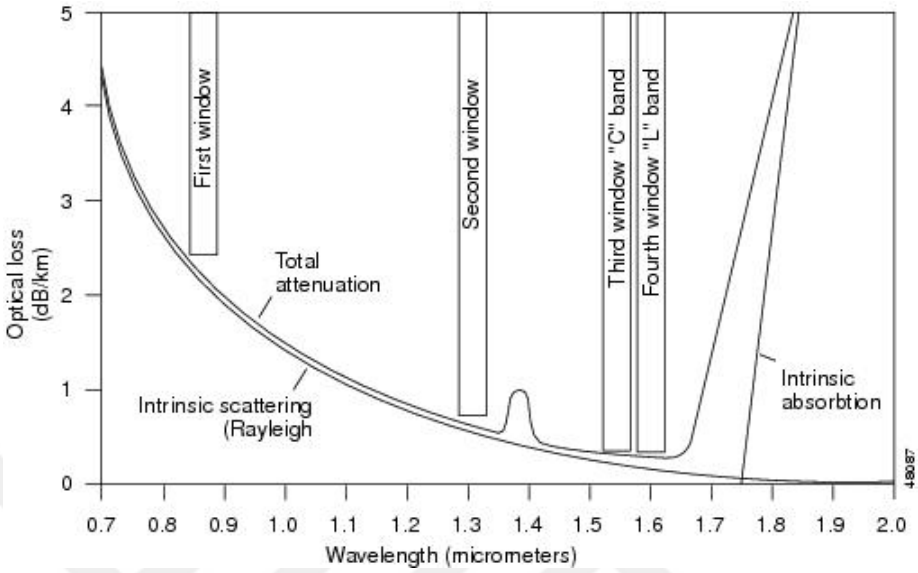

Figure 2.10: Single mode fiber attenuation vs. wavelength[35]

The wavelength interval denoted as C band in Figure 2.9 is the wavelength range at which fiber has the lowest attenuation. Hence, laser, modulator and photodetector in Figure 2.8 are all designed to operate at C band. Myriad of fiber optical components exist at C band thanks to widespread use of fiber in telecommunications industry.

2.3 Comparison of Measurement Methods

The oscillator under test subject to this thesis is an optical-bench optoelectronic oscillator(OEO) exhibiting an ultra low phase noise at a carrier of 10 GHz[7]. The system is not frequency locked to a stable source; therefore, center frequency of the oscillator is subject to drifts. The phase noises at 10 kHz offset at 10 GHz center frequency is as low as -140 dBc/Hz are reported in literature[7], thus; the system has a stringent sensitivity requirement to resolve such low phase noise.

First of all, direct measurement system, however simple, is not suitable to measure phase noise of a source described above. Referring to Figure 2.4, phase noise floor of spectrum analyzer E4440 is far worse than the targeted system measurement floor. Furthermore, because spectrum analyzer is not frequency locked to the oscillator under test, measurement is distorted by the frequency drift of the OEO. With all the disadvantages, since the spectrum analyzer is readily available at the laboratory, direct measurement method can be utilized as a validation or cross-check for the measurements obtained from the system described in this thesis. Hittite T2100 and HP83620B are both frequency-stabilized and exhibit large phase noise measureable with the spectrum analyzer[16][30]. Cross checking the measurements of these synthesizers obtained with a spectrum analyzer and/or the designed system with the datasheet values can serve as a validation methodology.

Phase locked loop and cross spectrum measurement methods both require a reference microwave source having a phase noise much lower than the oscillator under test. Such a source was not available at our laboratory; hence measurement methods are disregarded.

Finally, delay line frequency discriminator is concluded to be the most suitable system for the phase noise measurement of low phase noise sources exhibiting frequency drift. With the advantage of the optical fiber, system sensitivity can be boosted to resolve ultra low close in phase noise of the OEO. Furthermore, an integrator in the feedback loop to the variable phase shifter can easily result in zero voltage at the mixer and compensate the frequency and/or delay drifts. Design, calibration and characterization of the fiber optical delay line based frequency discriminator measurement system is elucidated in detail in subsequent chapters.

Chapter 3

System Design Description

3.1 System Description

The phase noise measurement system is a microwave photonics delay line frequency discriminator[32]. The system is designed to operate at 10 GHz, which is the frequency of the optoelectronic oscillator built in the laboratory. The input power is 4 dBm measured at the input of the directional coupler and monitored through P_{IN} in Figure 3.1. Selection for the input power is related to the optimum RF power injected into the delay line and described later.

Complete block diagram of the measurement system is illustrated in Figure 3.1. 10 dB directional couplers allow monitoring of microwave power spectrum at critical locations while the system is operating. Unless the −10 dB ports are connected to the spectrum analyzer, they are terminated in 50 Ω RF loads to prevent reflections. After tapping the input power, the signal is amplified to drive the electro-optical modulator RF input. A 3 dB microwave Wilkinson power divider splits power into delayed and non-delayed branches.

The delayed branch of the splitter drives the Mach-Zehnder type electro-optical intensity modulator, up-converting the input from microwave frequency, 10 GHz,

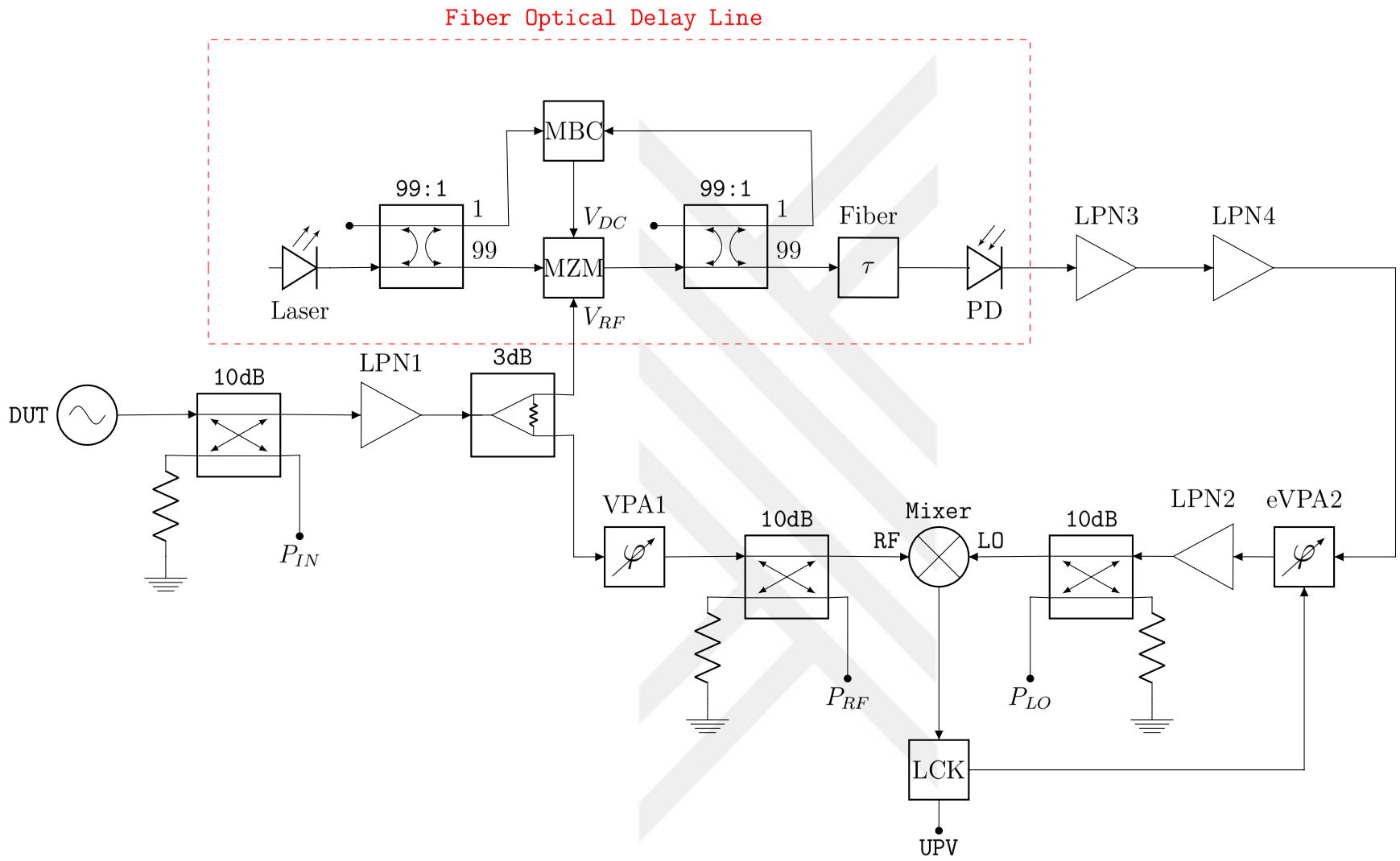

Figure 3.1: Block diagram of the measurement system. DUT: Device under test, LPN: Low Phase Noise Amplifier, 10 dB: 10 dB directional coupler, 3 dB: 3 dB power divider, VPA: Variable phase shifter, eVPA: Electronically controlled variable phase shifter, LCK: Lock circuitry, PD: photodetector, MZM: Mach-Zehnder Intensity Modulator, MBC: Photline MBC-AN MZM bias stabilizer circuit, UPV: Rohde-Schwarz UPV Audio Analyzer, Fiber: 5 km single mode fiber cable

to the optical frequency, 193.4 THz. Photline OEM MBC-AN circuit stabilizes DC bias of the modulator to the quadrature point and inhibits fluctuations in microwave power at the delay line output[36]. The modulated optical signal is injected into a 5 km long single mode optical fiber cable introducing 25 µs delay. The modulation side-bands are mixed at the photodetector to generate the microwave signal at the input microwave frequency of 10 GHz. The photodetector is a reverse-biased, high power InGaAs photodiode with an RF bandwidth of 24 GHz. To circumvent the microwave power loss during the electro-optical and opto-electrical conversions, low phase noise amplifiers are cascaded after the delay line. Electronically controlled variable phase shifter is driven with an OPAMP integrator circuit to bring the phase offset error at the mixer output to zero[37]. Another low phase noise amplifier is connected to compensate the loss due to the phase shifter.

The double balanced mixer is saturated at the RF and LO ports to function as a phase detector[31]. The microwave spectrum at the mixer arms are monitored with the 10 dB directional couplers. IF output of the mixer is connected to the custom designed circuit comprising several stages of OP-AMP circuits to filter, scale, amplify and integrate mixer output. With the filtering and amplification stage, 20 GHz part is attenuated and the measured signal is amplified to bring it above the noise floor of the data acquisition device. The scaling and integrator circuitry drives the phase shifter control input to stabilize the quadrature condition at the mixer RF and LO ports. Because electronically controlled phase shifter's microwave loss is a function of the control voltage, a mechanically controlled microwave phase shifter is connected at the non-delayed branch to bring the control voltage to the value used during the system calibration. The calibration procedure is described in the subsequent chapter.

UPV in Figure 3.1 is Rohde-Schwarz UPV Audio Analyzer data acquisition device[38]. Raw data is collected with a GPIB MATLAB software and processed offline in MATLAB.

3.2 Fiber Optical Delay Line Design and Characterization

Fiber optical delay line can be contemplated as a standalone, non reciprocal, two port microwave component and the design phase involves selecting appropriate set of optical components that would yield low noise and low loss delay line. The delay line is an externally intensity modulated direct detection microwave photonics link[39].

3.2.1 Fiber Optical Components

3.2.1.1 Laser

The laser source is a high power, low relative intensity noise (RIN), distributed feedback (DFB) laser operating at 1550.12 nm. High power lasers with low RIN yields better signal to noise ratio in microwave photonics links[40]. Hermetically sealed module operates at 5 V and draws 3 A current from the supply. The bottom of the module should be attached to a heat sink or a large thermal conducting metal body. Laser current source, thermoelectric cooler, optical isolator and temperature controller are also enclosed within the module. The output fiber pigtail is a single mode polarization maintaining fiber aligned to slow axis. Laser parameters are provided in Table 3.1 and low frequency relative intensity noise is illustrated in Figure 3.2.

Table 3.1: Laser parameters.

Parameter	**Value**
Optical Output Power [mW]	100
Linewidth [kHz]	170
RIN 50 MHz-18 GHz [dB/Hz]	−150
Cold Start Settling Time [s]	30

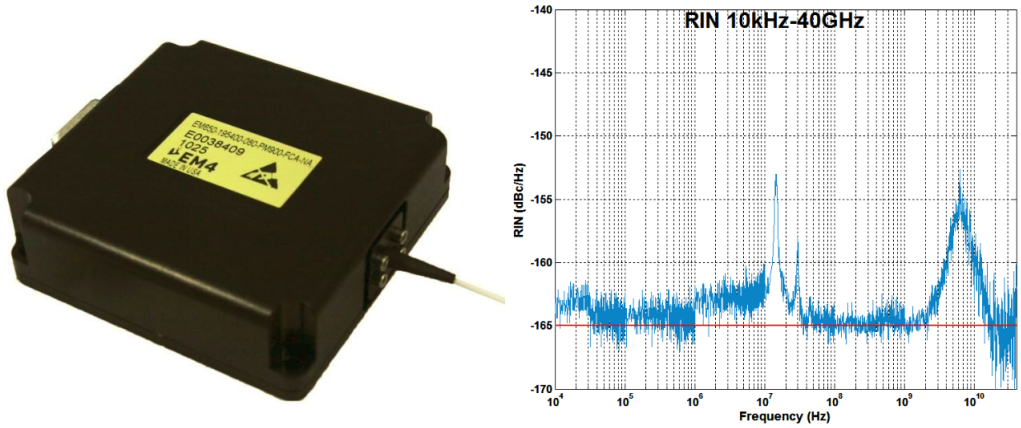

Figure 3.2: Laser module and relative intensity noise for 10 kHz to 40 GHz

3.2.1.2 Mach-Zehnder Intensity Modulator

Mach-Zehnder type intensity modulator modulates the optical signal at the frequency of 193.4 THz with the microwave signal at 10 GHz. The modulator in the system is manufactured on a z-cut $LiNbO_3$ crystal. The optical input is injected through a PANDA polarization maintaining single mode optical fiber aligned to slow axis; RF and DC inputs are applied on separate electrodes. Figure 3.3 illustrates single-arm drive modulator structure.

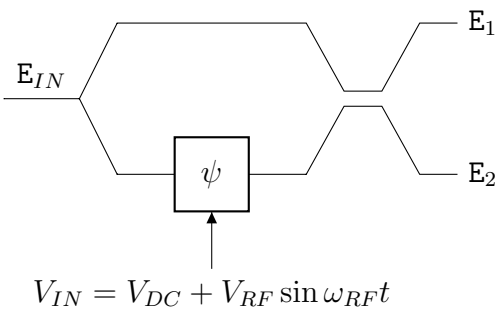

Figure 3.3: Mach-Zehnder intensity modulator with single arm drive[41]. E_{IN}: monochromatic optical input, $E_{1,2}$: out of phase output fields, ψ: phase shift incurred by RF input signal

Assuming input monochromatic optical field, transfer function of the modulator is written as[41]

$$\begin{bmatrix} E_1 \\ E_2 \end{bmatrix} = C_1 e^{j\omega t} \begin{bmatrix} e^{j\psi} - 1 \\ je^{j\psi} + j \end{bmatrix} \tag{3.1}$$

where ψ denotes optical phase shift incurred by the RF drive and C_1 denotes the constant to account for modulator losses. If we attach a photodetector at each arm of the modulator, the photocurrents would proportional to

$$I_{1,2} \propto (1 \mp \cos\psi) \tag{3.2}$$

where $I_{1,2}$ represents photo-currents at each arm. Inserted phase shift, ψ, is related to RF drive with the half wave voltage of the modulator through[42]

$$\psi = \psi_{DC} + \psi_{RF} sin(\omega_{RF} t) \tag{3.3}$$

$$\psi_{DC} = \frac{\pi V_{DC}}{V_{\pi_{DC}}} \tag{3.4}$$

$$\psi_{RF} = \frac{\pi V_{RF}}{V_{\pi_{RF}}} \tag{3.5}$$

$V_{\pi_{DC}}$ and $V_{\pi_{RF}}$ of the half wave voltage of the modulator at DC and RF are defined as the required voltage to generate π radians phase shift at the modulator arm[41]. Half wave voltage of the modulator is the vital parameter for the system design[10][32]. Accurate characterization of the half wave voltage at the working microwave frequency bears importance due to the increase in half wave voltage with the increasing frequency[43].

Output photo-current spectrum can be obtained using Jacobi-Anger expansion[42]

$$\begin{aligned} I_{1,2} \propto 1 \mp \cos\psi_{DC} &\left[J_0(\psi_{RF}) + 2\sum_{n=1}^{\infty} J_{2n}(\psi_{RF}) \cos 2n\omega_{RF} t \right] \\ \pm \sin\psi_{DC} &\left[2\sum_{m=1}^{\infty} J_{2m-1}(\psi_{RF}) \sin(2m-1)\omega_{RF} t \right] \end{aligned} \tag{3.6}$$

The spectrum of the photocurrent includes many harmonics of the fundamental frequency and the amplitudes of the harmonics depend on the DC bias of the

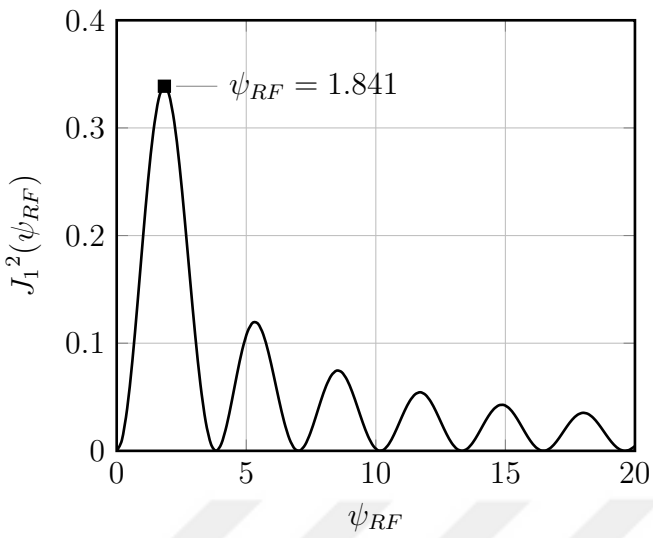

Figure 3.4: Nonlinear response of Mach-Zehnder modulator. Maximum RF gain is achieved at $\psi_{RF} = 1.841$[8].

modulator. For the quadrature condition, $\psi_{DC} = \pi/2$, the second order harmonics vanish

$$I_{1,2} \propto \pm \left[2 \sum_{m=1}^{\infty} J_{2m-1}(\psi_{RF}) \sin{(2m-1)\omega_{RF} t} \right] \tag{3.7}$$

$$I_{c_{1,2}} \propto J_1(\psi_{RF}) \sin \omega_{RF} t \tag{3.8}$$

Two important conclusions are drawn from Figure 3.4 and equation 3.8.

- RF loss of the delay line is a nonlinear function of input RF amplitude. The optimum RF power for the maximum gain occurs at $\psi_{RF} = 1.841$ corresponding to $V_{RF} = 0.586 V_\pi$[8]. Low half wave voltage modulators are preferable to achieve optimum RF power with a reasonable modulator driver amplifier. $V_\pi = 3.1\,\mathrm{V}$ for our modulator measured using the two-tone RF mixing method as described later. Then, optimum modulation index would have been achieved with 15.188 dBm input RF power. However, modulation index is practically selected less than the maximum because of difficulty in obtaining bias stabilization and the maximum modulation index at the same time[8]. The modulation index is set to 1.134, slightly less than 1.841, the optimum index. Modulator RF drive power budget is given in Figure 3.5.

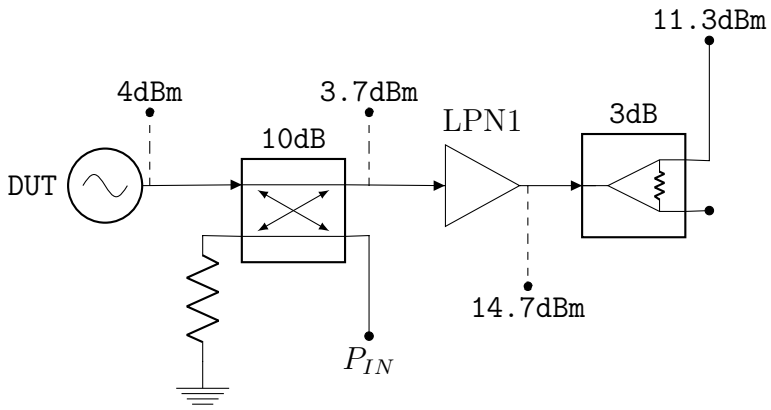

Figure 3.5: Microwave power budget to achieve modulation index of 1.134 in the modulator. −10 dB coupled port of the directional coupler was used to monitor the powers without disrupting the system operation.

- Half wave voltage of the modulator not only affects attainable modulation index but also RF loss of the delay line. For small signal RF, RF loss is inversely proportional to the square of the half wave voltage[10]; hence low half wave voltage is desirable to achieve low loss delay line.

3.2.1.2.1 Half wave voltage characterization Half wave voltage of different modulators are measured using the two-tone microwave measurement method[44]. The two tone measurement system is quite reliable and requires no calibration of photodetector frequency response. The measurement method is depicted in Figure 3.6.

The two tone input to the modulator is

$$\psi = \psi_1 \sin(\omega_1 t) + \psi_2 \sin(\omega_2 t) \tag{3.9}$$

$$\psi_1 = \frac{\pi V_1}{V_\pi} \tag{3.10}$$

$$\psi_2 = \frac{\pi V_2}{V_\pi} \tag{3.11}$$

where it is assumed that half wave voltage is constant in $[f_1, f_2]$ and $V_1 = V_2 = V_{IN} \ll V_\pi$ are selected. In the measurement system $f_1 = 10\,\text{GHz}$ and $f_2 = 10.05\,\text{GHz}$ are input frequencies. The spectra of output photocurrent is then

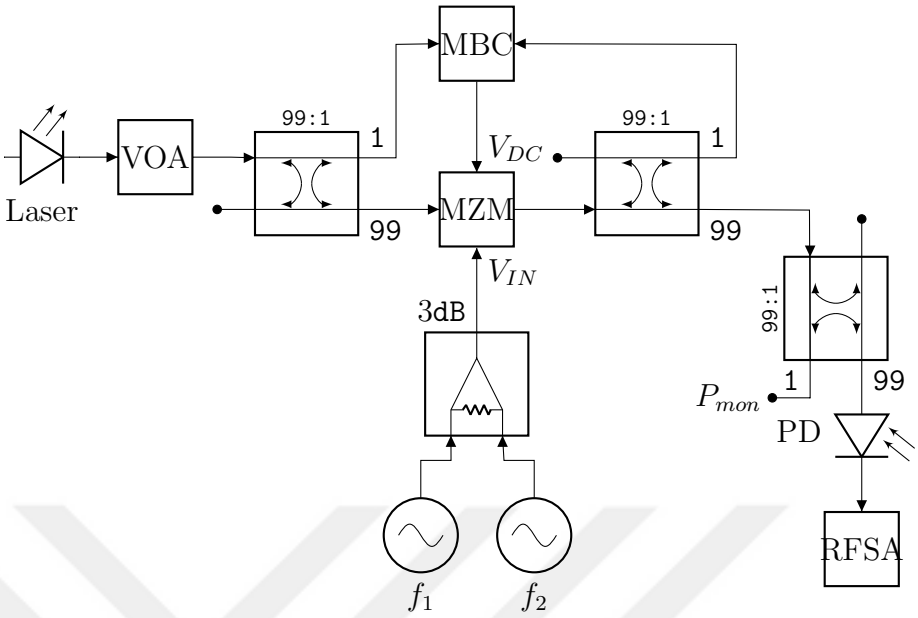

Figure 3.6: Two-tone V_π measurement system. VOA: Variable optical attenuator, MZM: Mach-Zehnder Modulator, MBC: Modulator bias controller, 99:1: Optical X coupler with 99/1 coupling ratio, 3 dB: Microwave power combiner to combine microwave frequency f_1 and f_2 at the modulator input, PD: Photodetector, RFSA: RF spectrum analyzer.

calculated as

$$
\begin{aligned}
I \propto \sin(\psi_{DC})[&2J_0(\psi_2)J_1(\psi_1)\sin(\omega_1 t)+\\
&2J_2(\psi_2)J_1(\psi_1)\cos(2\omega_2-\omega_1)t-\\
&J_2(\psi_2)J_1(\psi_1)\cos(2\omega_2+\omega_1)t\\
&2J_0(\psi_1)J_1(\psi_1)\sin(\omega_2 t)+\\
&2J_2(\psi_1)J_1(\psi_2)\cos(2\omega_1-\omega_2)t+\\
&J_2(\psi_1)J_1(\psi_2)\cos(2\omega_2+\omega_1)t+\ldots]+\\
\cos(\psi_{DC})[&J_0(\psi_1)J_0(\psi_2)+\\
&2J_0(\psi_1)J_2(\psi_2)\sin(2\omega_2 t)+\\
&2J_2(\psi_2)J_1(\psi_1)\cos(2\omega_1-2\omega_2)t+\\
&2J_0(\psi_2)J_2(\psi_1)\sin(2\omega_1 t)+\\
&2J_2(\psi_2)J_1(\psi_1)\cos(2\omega_1+2\omega_2)t+\\
&2J_1(\psi_2)J_1(\psi_1)\cos(\omega_1-\omega_2)t+\\
&2J_1(\psi_1)J_1(\psi_2)\cos(\omega_1+\omega_2)t+\ldots]
\end{aligned}
\tag{3.12}
$$

Note that $\psi_1 = \psi_2$ and at the quadrature condition $\psi_{DC} = \pi/2$, $\cos(\psi_{DC})$ terms vanish. The terms of interest are fundamental and inter-modulation frequencies

$$I(\omega_1) = I(\omega_2) \propto 2J_0(\psi_2)J_1(\psi_1) \tag{3.13}$$

$$I(2\omega_2 - \omega_1) = I(2\omega_1 - \omega_2) \propto 2J_2(\psi_2)J_1(\psi_1) \tag{3.14}$$

Using the small argument approximation for Bessel functions given in 2.20, closed form solution can be obtained for the half wave voltage

$$\psi_1 = \psi_2 = \psi = \frac{\pi V_{in}}{V_\pi} \tag{3.15}$$

$$\frac{P_{fun}}{P_{imd}} = \frac{J_0^2(\psi)J_1^2(\psi)}{J_2^2(\psi)J_1^2(\psi)} \approx \frac{8V_\pi^4}{\pi^4 V_{in}^4} \tag{3.16}$$

$$V_\pi = \frac{\pi V_{IN}}{2\sqrt{2}} \left(\frac{P_{fun}}{P_{imd}}\right)^{0.25} \tag{3.17}$$

Since spectrum analyzer measurements are in dBm, equation 3.17 can be put in a more useful form

$$V_\pi = \frac{\pi V_{IN}}{2\sqrt{2}} 10^{\frac{P_{fun} - P_{imd}}{40}} \tag{3.18}$$

V_{IN} can be easily measured at the output of the Wilkinson combiner, including the coaxial cable from the output of the Wilkinson divider to the input of the modulator. The power at the fundamental frequency P_{fun} and the inter-modulation frequency P_{imd} can also be obtained with the spectrum analyzer. Because V_π is obtained by taking the ratio of the powers, the calibration is not required for the RF response of the photodetector, assuming frequency response is flat within the bandwidth, 150 MHz in this case.

For proper measurement several points should be addressed

- Linearity of the delay line must be limited by the modulator but not the photodetector. The simplest way to verify this is by varying the optical power onto the photodetector. The power at the fundamental frequency and the inter-modulation frequency increase by the same ratio; hence photocurrent would have no effect on the measured value of the half wave voltage. We verified this by inserting a polarization maintaining variable

optical attenuator after the laser to control the photocurrent and observed no change in the measured value with changing photocurrent.

- Spectrum analyzer should have better linearity than the modulator. Simple method to verify this is to measure the inter-modulation products after the Wilkinson power combiner in Figure 3.6 with the input powers adjusted to expected output power at the fundamental frequency. We measured 90 dBc with -10 dBm input power at f_1 and f_2 allowing measurements of half wave voltages up to 19.7 V.

- Another issue is placing a post amplifier like the one in figure 2.9. Inter-modulation products due to non-linearity in the amplifier should be lower than the ones due to modulator which might prove difficult to achieve in practice. The simple methodology described in the first item can also be utilized for this item to verify that non-linearity in the delay line is due to modulator but not the amplifier. Increasing the link gain by 1 dB by increasing the optical power on the photodetector would not change the fundamental to inter-modulation ratio should the delay line non-linearity is modulator limited. If it was amplifier limited, inter-modulation products would increase by 3 dB; hence the ratio would not be the same.

- As discussed before, DC bias of the Mach-Zehnder modulators are subject to slow drifts fluctuating the delay line RF loss during the measurement. To prevent any fluctuation while measuring inter-modulation and fundamental frequency powers, MBC-AN analog bias stabilizer circuitry was inserted to lock the modulator bias to the quadrature to ensure that delay line gain is stabilized against drifts.

V_π of two commercial-off-the-shelf modulators are measured with the method and the results are presented. The input powers to the modulator are set to -10 dBm for $f_1 = f_0$ GHz and $f_2 = f_0 + 0.05$ GHz where f_0 is swept from 9 GHz to 10 GHz with 100 MHz step size. The power in the lower inter-modulation sideband is recorded for the calculation. For the first modulator, power measurements are tabulated in Table 3.2. Only one digit is shown to fit the data to table.

Measured half wave voltage is illustrated in Figure 3.7. At 10 GHz, $V_\pi = 3.087\,\mathrm{V}$.

To further increase the confidence in measurements, RF input power was set to $[-15, -10, -5, 0, 5, 10]$ dBm at 10 GHz and the ratio of the power in fundamental frequency to the power of lower inter-modulation sideband is recorded for each input RF power. The recorded value is compared to the theoretical calculation of equation 3.16 for the measured half wave voltage $V_\pi = 3.087\,\mathrm{V}$. The plot shown in Figure 3.8 indicates agreement between measurement and the theoretical calculation.

Identical measurements are carried out for modulator two and the results are given in Table 3.3 and Figures 3.9 and 3.10. Half wave of voltage of the modulator two is $V_\pi = 7.51\,\mathrm{V}$ at 10 GHz. Since the half wave voltage of the modulator one is much smaller than that of modulator two, modulator one is employed in the system.

Table 3.2: Power measurements for modulator one

Frequency[GHz]	9	9.1	9.2	9.3	9.4	9.5	9.6	9.7	9.8	9.9	10
P_{fun}[dBm]	-29.4	-29.0	-29.4	-29.5	-28.9	-29.8	-29.1	-29.4	-29.3	-29.2	-29.2
P_{imd}[dBm]	-88.6	-87.7	-88.7	-88.2	-88.3	-88.7	-87.9	-88.5	-87.7	-87.7	-86.9

Table 3.3: Power measurements for modulator two

Frequency[GHz]	9	9.1	9.2	9.3	9.4	9.5	9.6	9.7	9.8	9.9	10
P_{fun}[dBm]	-35.9	-35.4	-35.8	-35.8	-35.3	-36.0	-35.4	-35.7	-36.0	-35.7	-35.5
P_{imd}[dBm]	-110.5	-109.5	-110.2	-109.7	-109.9	-109.8	-109.4	-110.8	-109.6	-110.6	-109.1

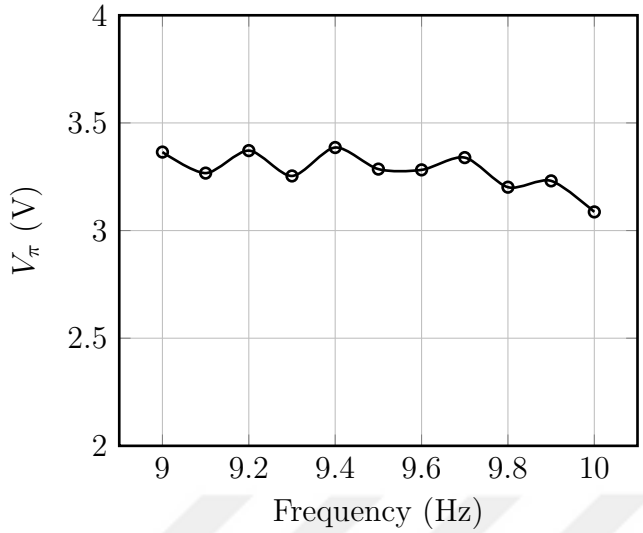

Figure 3.7: Half wave voltage measurement for modulator one is illustrated.

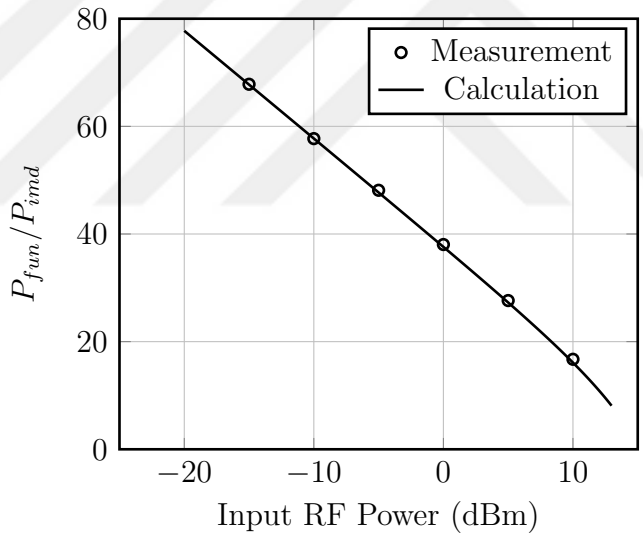

Figure 3.8: Comparing theoretical sideband to carrier ratio to measured values for modulator one.

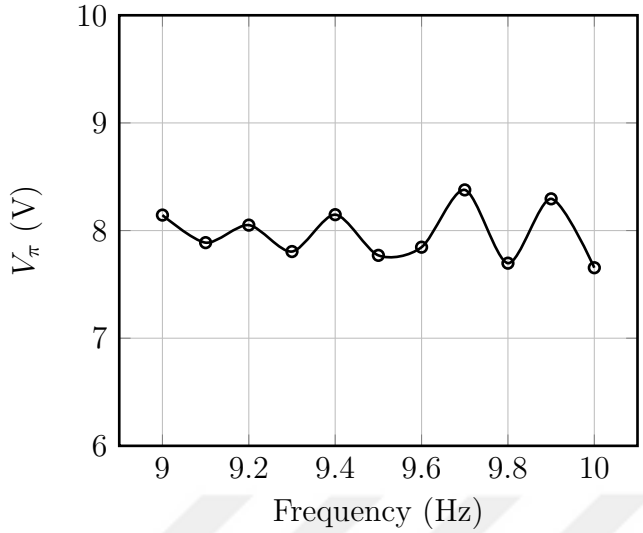

Figure 3.9: Half wave voltage measurement for modulator two is illustrated.

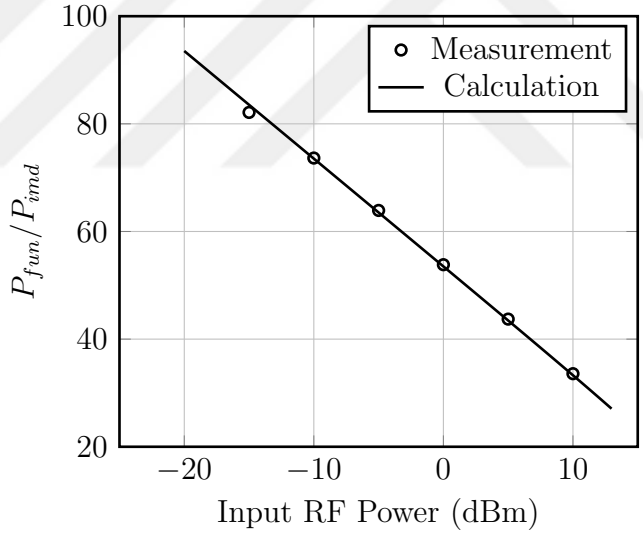

Figure 3.10: Comparing theoretical sideband to carrier ratio to measured values for modulator two.

3.2.1.3 Single Mode Fiber Cable

The component realizing the delay is 5 km single mode optical fiber and the structure is illustrated in Figure 3.11.

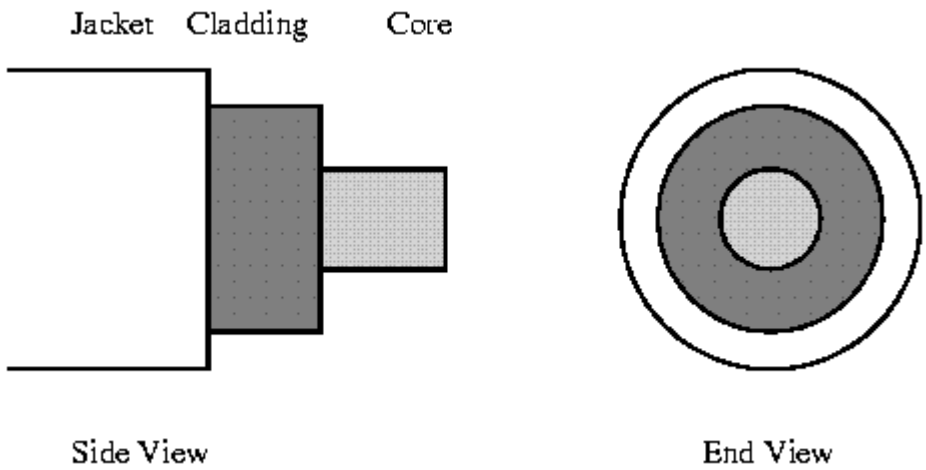

Figure 3.11: Core, cladding and coating of the single mode optical fiber, excerpt from[45]

Specifications of the fiber is enumerated in Table 3.4. The length of the delay is measured using optical time domain reflectometer(OTDR) device and found to be 5048 m. The measurement is illustrated in Figure 3.12.

Table 3.4: Specifications of the optical fiber

Parameter	**Value**
Core Diameter[µm]	8.2
Cladding Diameter[µm]	125
Coating Diameter[µm]	242
Loss(at 1550 nm)[dB/km]	0.2
Refractive Index of Core	1.4682

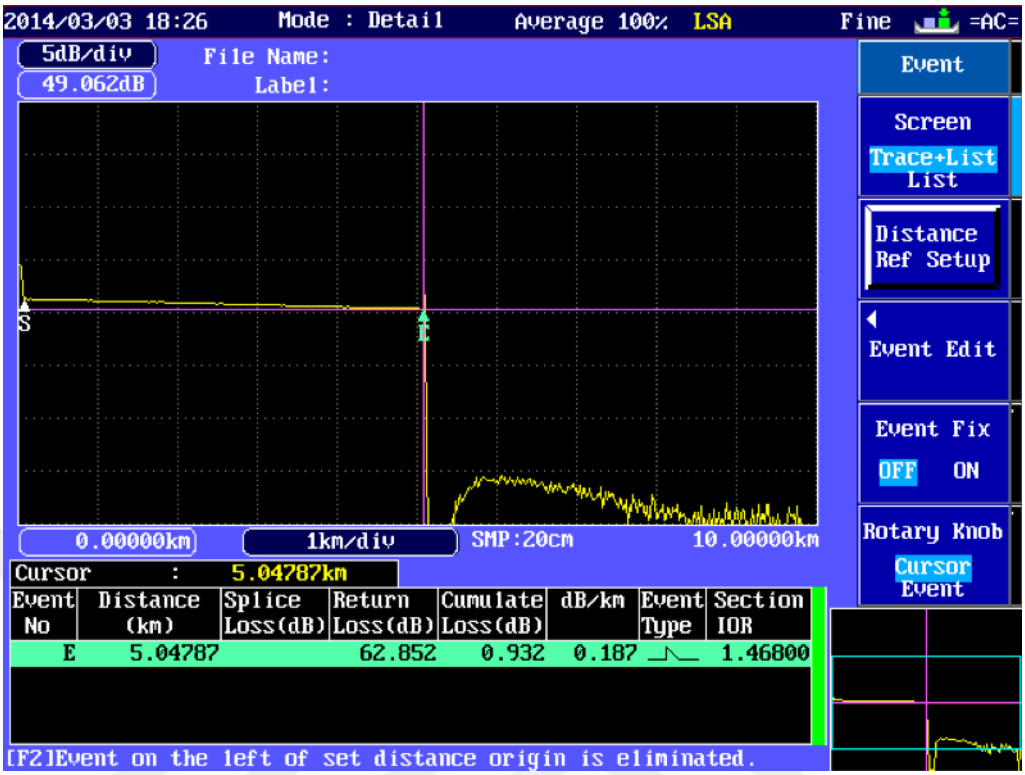

Figure 3.12: OTDR measurement of the optical fiber

Using the distance measurement in Figure 3.12 and refractive index in Table 3.4, the realized delay is calculated as

$$\tau = \frac{n \cdot L}{c} = \frac{1.468 \cdot 5048}{2.998e8} = 24.7\,\mu\text{s} \tag{3.19}$$

3.2.1.4 Photodetector

The photodetector is a high power, wide RF bandwidth, hermetically sealed, InGaAs PIN diode reverse biased to 6 V with 4 batteries. The optical input is a single mode fiber and the output is RF K connector. Photodetector can work linearly for incident optical powers up to 27 mW. High power handling of the photodetector is of utmost important for analog optical delay lines to achieve high signal to noise ratio[10]. RF 3 dB bandwidth illustrated in Figure 3.13 is approximately 24 GHz.

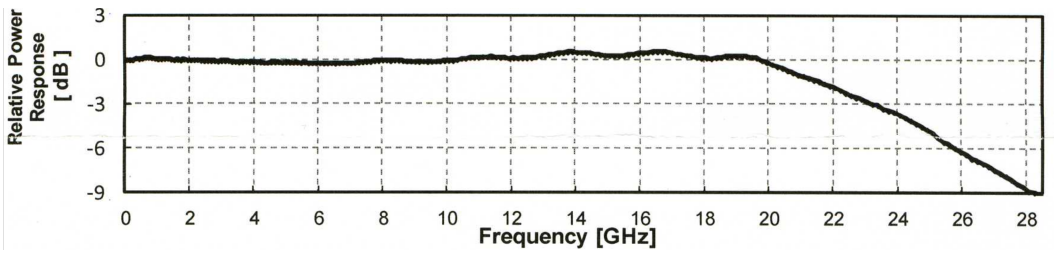

Figure 3.13: RF bandwidth of photodetector

Table 3.5: Photodetector specifications.

Parameter	Value
-3dB Bandwidth [GHz]	22.7
DC Responsivity [A/W]	0.73
Dark Current at 5 V[nA]	12
Optical return loss[dB]	40

3.2.2 RF Bandwidth Characterization

As discussed before, microwave photonics delay line can be treated as a nonreciprocal, two port microwave component. The delay line is linear when the driving microwave signal is much smaller than the half wave voltage of the modulator. Frequency response of the linear microwave system is measured with a calibrated network analyzer. Measurement setup is shown in Figure 3.14.

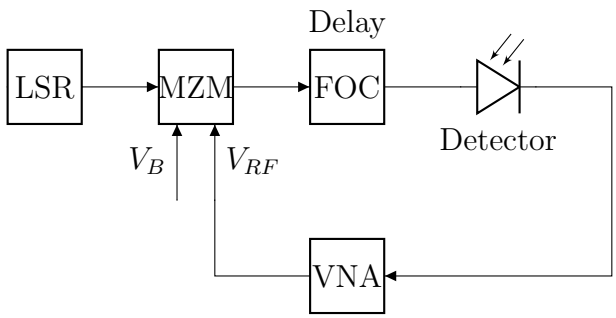

Figure 3.14: RF bandwidth measurement of the delay line. LSR: Laser source, MZM: Mach-Zehnder intensity modulator, FOC: Fiber optical cable, VNA: Vector network analyzer

VNA in Figure 3.14 is the calibrated Agilent E8361C network analyzer. DC

bias of the modulator is set to the quadrature condition for linear operation. Two measurements are recorded for 5 km single mode and 20 km near zero dispersion shifted fibers and results are illustrated in Figures 3.15 and 3.16. The sharp null at around 21 GHz in both Figures in 3.15 and 3.16 is due to chromatic dispersion based RF power fading in the single mode fiber[46].

The frequency response of the delay line is modified when the third term of the propagation constant is taken into account[46].

$$I_{pd} \propto \cos\left(\frac{1}{2}\beta_2 L\omega_{RF}^2\right) \tag{3.20}$$

where β_2 is the third term of the Taylor expansion of the propagation constant in ps^2/km, L is the fiber length in kilometers and ω_{RF} is angular microwave frequency. Since the group delay in the fiber is frequency dependent, at a certain frequency, the phase difference between the intensity modulated sidebands reaches 180 deg and intensity modulation is completely converted to phase modulation. The theoretical plot in Figure 3.15 is for $\beta_2 = 34.6$ ps^2/km and in Figure 3.16 is for $\beta_2 = 8.4$ ps^2/km. Near zero dispersion fiber is a specialty of fiber with the dispersion parameter is designed to be closer to zero and has an advantage for wideband fiber optical links. To circumvent chromatic dispersion effects, laser source can be selected as 1310 nm, a short length of dispersion compensation fiber can be spliced to cancel out the dispersion in the single mode fiber or single sideband modulation can be implemented instead of double sideband modulation[47].

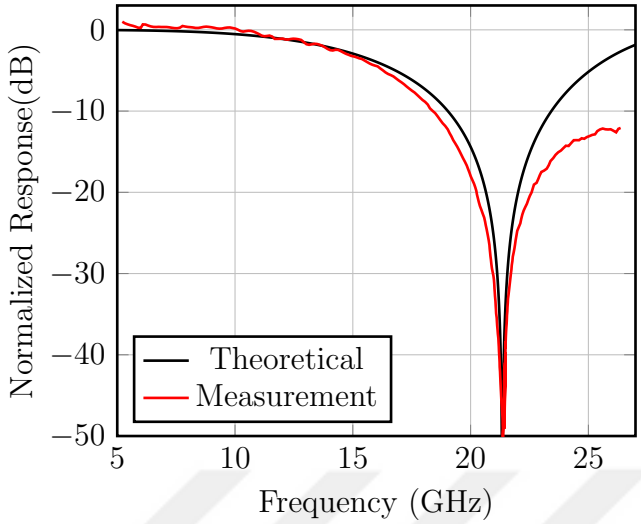

Figure 3.15: RF bandwidth measurement with 5 km single mode fiber delay

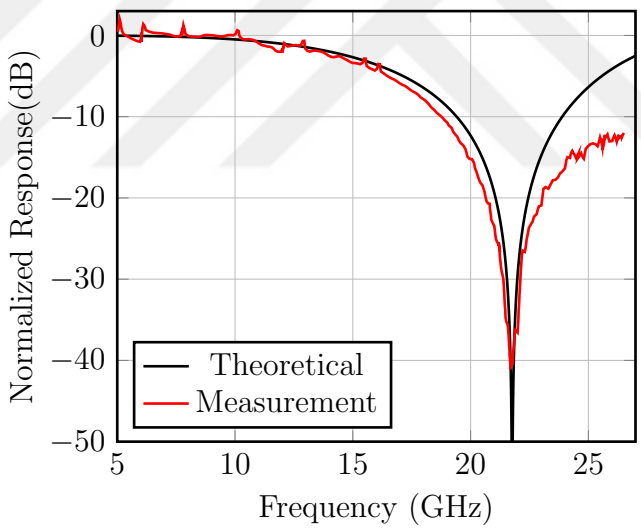

Figure 3.16: RF bandwidth measurement with 20 km near zero dispersion shifted fiber delay

3.2.3 Optical Power Saturation Characterization

Linear input output relationship in the optical fiber is not preserved when the optical power injected into the fiber stimulates nonlinear interactions between the incident electric field and the fiber media, silica in this case[48]. Since the system has a 170 kHz narrow linewidth laser source and a long fiber cable, Stimulated Brillouin Scattering(SBS) is the dominant effect limiting the optical power into the fiber[49]. We analyzed SBS effect experimentally and measured SBS threshold power of 5 km single mode(SMF) and 20 km near-zero dispersion(NZDSF) fibers. The measurement setup is illustrated in Figure 3.17.

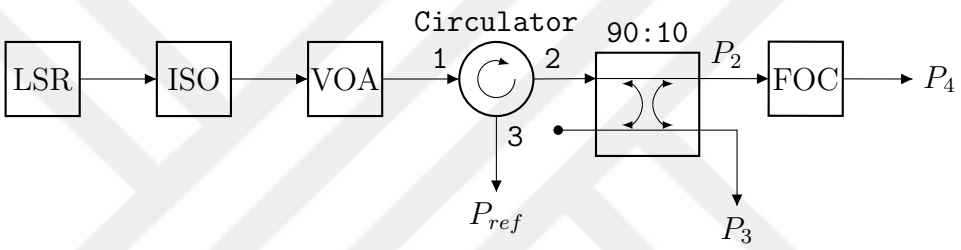

Figure 3.17: SBS threshold power measurement setup for fiber optical fiber[49]. LSR: Laser source, ISO: Optical isolator, VOA: Variable optical attenuator, FOC: Fiber optical cable

In Figure 3.17, laser source is the laser described in Section 2.2.1.1. The isolator after the laser ensures that no reflected power destabilizes laser. Variable optical attenuator controls the injected power to the fiber. The circulator directs reflected power to the P_{ref} port. The coupler ratio $P_2/P_3 = 9.1$ and allows monitoring of the injected power without removing the fiber cable. Insertion loss of the coupler is -0.67 dB, insertion loss of the circulator from port 2 to port 3 is -0.69 dB. Power measurements are recorded with an optical power meter.

Measurement for 5 km fiber is illustrated in Figure 3.18. The result is typical for a single mode fiber [50]. Up to the threshold incident power value of 11 dBm, the reflected and transmitted power increase linearly, hence fiber is operating in the linear regime. When SBS is excited, reflected power increases dramatically and transmitted power saturates. At 14 dBm incident power, transmitted power can no longer increases and stays constant at 13 dBm.

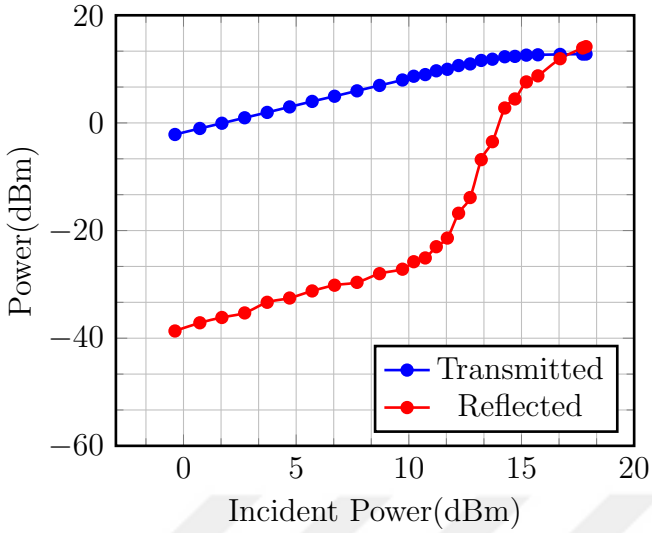

Figure 3.18: SBS threshold measurement for 5 km SMF

Similarly, Figure 3.19 illustrates non-linearity in the near zero dispersion shifted fiber. The threshold value for SBS excitation is measured to be 9 dBm. Transmitted power cannot increase beyond 6.5 dBm with 20 km NZDS fiber. Saturation due to SBS effect happens at lower power levels when the fiber length is increased. At our system, power in the detector is 6.13 dBm transmitted through 5 km SMF. Notice that for the same power level, 20 km NZDS fiber is saturated.

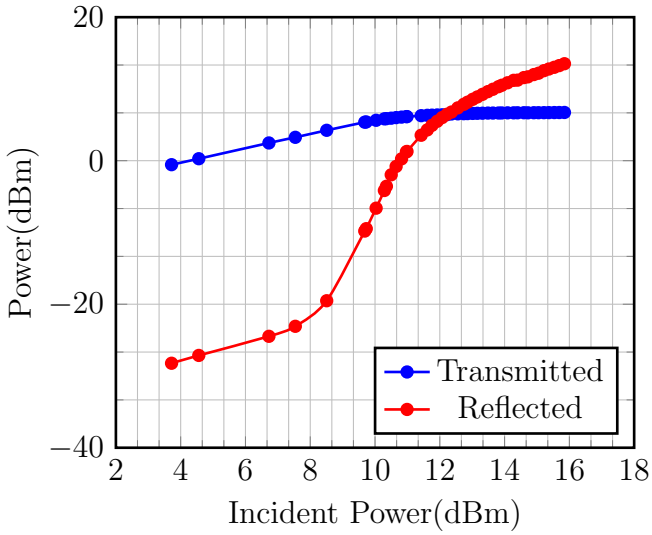

Figure 3.19: SBS threshold measurement for 20 km SMF

3.3 Microwave Link Design and Characterization

3.3.1 Low Phase Noise Amplifiers

As it is recognized from Figure 3.1, four amplifiers are employed in the system. LPN1 functions like a modulator driver whereas LPN2, LPN3, LPN4 are post-amplifiers to drive the LO port of the double balanced mixer to the nominal value. Microwave amplifiers are selected to be low phase noise amplifiers having an extremely low residual additive phase noise in order not to interfere with the phase of the signal under test. Residual phase noise datasheet values are given in Figures 3.20 and 3.21 and other specifications are given in Tables 3.6, 3.7 for LNP1,LPN3 and LPN2,LPN4 respectively. The residual phase noise of the amplifiers is much smaller than close in phase noise of optoelectronic oscillators discussed in literature[51]. Amplifiers are hermetically sealed and operate at 7 V supply. RF input and output ports are matched to 50 Ω.

Table 3.6: Specifications for LPN1 and LPN3.

Parameter	**Value**
Frequency Range[GHz]	7-11
Gain[dB]	9
Noise Figure	6
P_{1dB}Out[dBm]	22

Table 3.7: Specifications for LPN2 and LPN4.

Parameter	**Value**
Frequency Range[GHz]	6-12
Gain[dB]	11
Noise Figure	4.5
P_{1dB}Out[dBm]	20

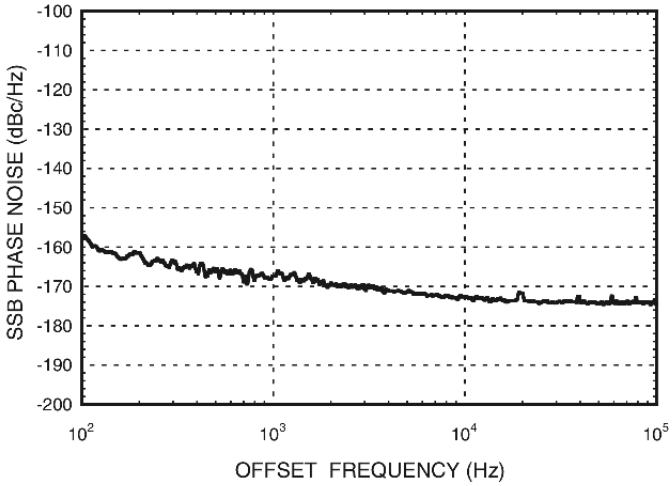

Figure 3.20: Residual phase noise of LPN1 and LPN3 at $P_{out} = 10\,\text{dBm}$

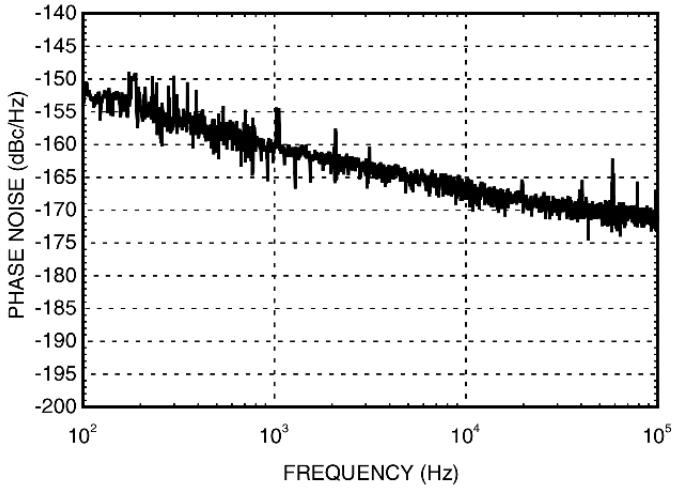

Figure 3.21: Residual phase noise of LPN1 and LPN3 at $P_{out} = 10\,\text{dBm}$ at $9\,\text{GHz}$

3.3.2 Variable Phase Shifter

From figure 3.1, one mechanical, VPA1, and one electronic, eVPA, variable phase shifters are integrated to the system. Phase shifters are used to maintain quadrature condition at the mixer arms. The signal at the mixer output in figure 3.1 drives the control voltage of the phase shifter through an integrator to reduce the

phase error to zero[37].

Specifications for electronically controlled phase shifter are provided in Table 3.8. Normalized phase shift against the control voltage is illustrated in Figure 3.22 and change in the insertion loss for changing the control voltage is provided in Figure 3.23. Mechanical phase shifter compensates for the change in the insertion loss by manually bringing the phase error to the same control voltage at which the calibration procedure was carried out.

Table 3.8: Specifications for electronically controlled phase shifter.

Parameter	**Value**
Phase Shift Range at 10 to 15 GHz[deg]	600
Insertion Loss[dB]	10
Control Voltage Range[V]	0-5
Modulation Bandwidth[MHz]	50
Phase Voltage Sensitivity[deg/V]	120

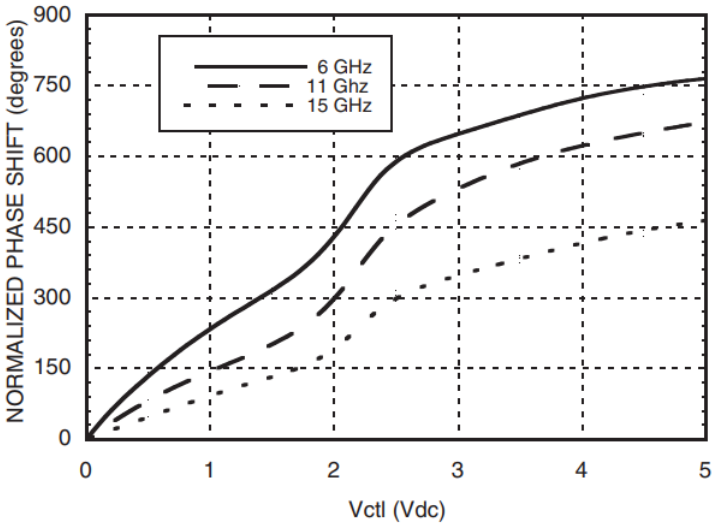

Figure 3.22: Phase shift vs. control voltage

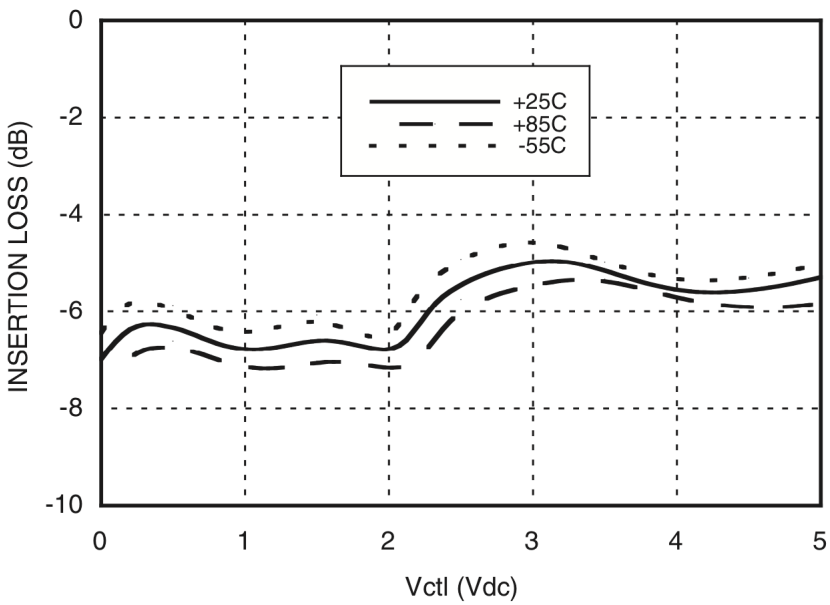

Figure 3.23: Control voltage vs. insertion loss

3.3.3 Double Balanced Mixer as a Phase Detector

The mixer operating as a phase detector is a hermetically sealed double balanced mixer with a low conversion loss and high isolation between the ports[52]. The specifications of the mixer are given in Table 3.9.

Table 3.9: Specifications for the double balanced mixer.

Parameter	**Value**
LO,RF Bandwidth[GHz]	2-20
IF Bandwidth[GHz]	DC-2
Conversion Loss[dB]	7
Isolation LO-RF[dB]	45
Isolation LO-IF[dB]	20
Isolation RF-IF[dB]	-30
Input 1dB Compression[dBm]	3
LO Drive Level[dBm]	10-13

To operate the mixer as a phase detector, RF port must be driven into

saturation[31]. In Table 3.9, compression power is given to be 3 dBm. We performed similar measurement given in [52] to verify that the mixer is saturated at calibrated power levels at the RF and LO ports. The simple measurement setup is illustrated in Figure 3.24.

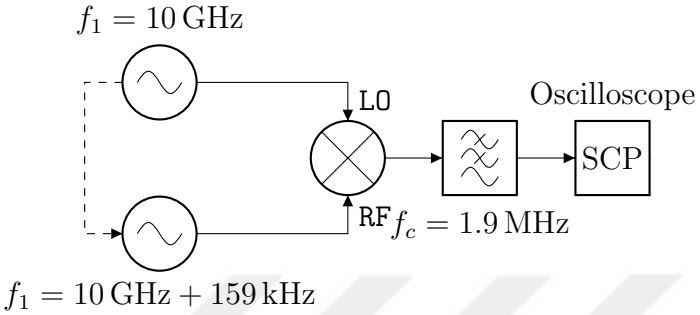

Figure 3.24: Mixer saturation power measurement setup, excerpt from[52].

In Figure 3.24, the power in LO port is fixed to 13 dBm as the nominal LO power specified in Table 3.9. Power in the RF port is varied from −4 dBm to 10 dBm and peak to peak voltage is recorded for each power. The result is given in Figure 3.25.

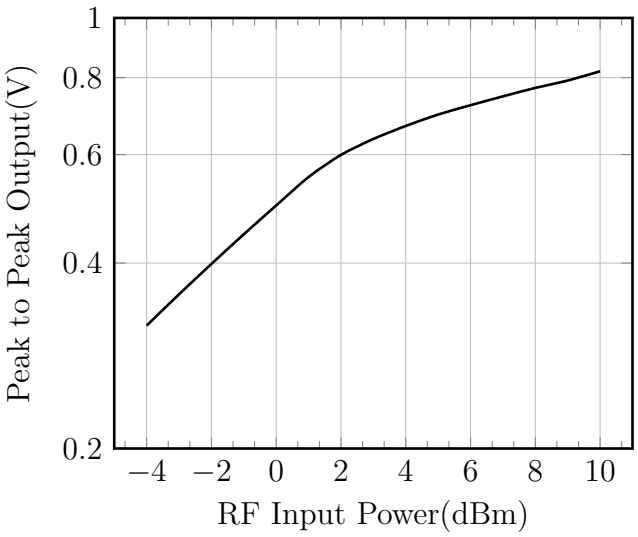

Figure 3.25: Mixer saturation power measurement.

The mixer starts to saturate at 3 dBm as given in Figure 3.9. However, peak to peak voltage continues to increase with increasing RF power. Hence, using the mixer with high power at both RF and LO ports increases the system

sensitivity[52]. In the setup given in Figure 3.1, the mixer LO power is selected as nominal power of 13 dBm and RF power is 9 dBm to ensure the saturation. Higher power was not achievable without additional amplification in the non-delayed branch in the system given in Figure 3.1.

3.3.4 Quadrature Locking Circuit

As discussed in Chapter 2, relative phase difference between RF and LO arms of the mixer must be maintained at 90 deg to utilize mixer as a phase detector. Although phase difference could have been adjusted to quadrature by manually steering the knob of the manual phase shifter to bring mixer DC output to zero, the system cannot maintain the quadrature state because of fluctuations in the fiber delay and laser frequency[52]. An active control of the relative phase difference between the two arms is implemented using an OP-AMP based analog integrator and an electronically controlled analog phase shifter[37].

Complete circuit schematics is illustrated in Figure 3.26. The circuit shown in the top of Figure 3.26 is a low noise positive supply circuit based on the low noise TPS7A4700 voltage regulator. 20 V input is converted and filtered down to 15 V which is the positive supply voltage for the OP-AMPs in the circuit. Similarly, the circuit on the bottom of Figure 3.26 is a low noise negative voltage supply circuit based on TPS7A3301 voltage regulator. −20 V is again filtered to −15 V for negative supply voltages of OP-AMPS. Input bias voltages are supplied with 2.2 µF capacitive feed-trough filters.

The circuitry given in the middle of Figure 3.26 illustrates the OP-AMP circuit design for amplification, integration and offsetting the mixer output voltage to scale to the phase shifter control voltage.

The first stage in Figure 3.27 provides −5.6 V voltage gain to amplify noise above signal analyzer's noise floor and the second stage integrates signal with a 100 µF capacitor. If the control loop enters into a positive feedback state, where the integrator output increases or decreases until OP-AMP hits saturation, the

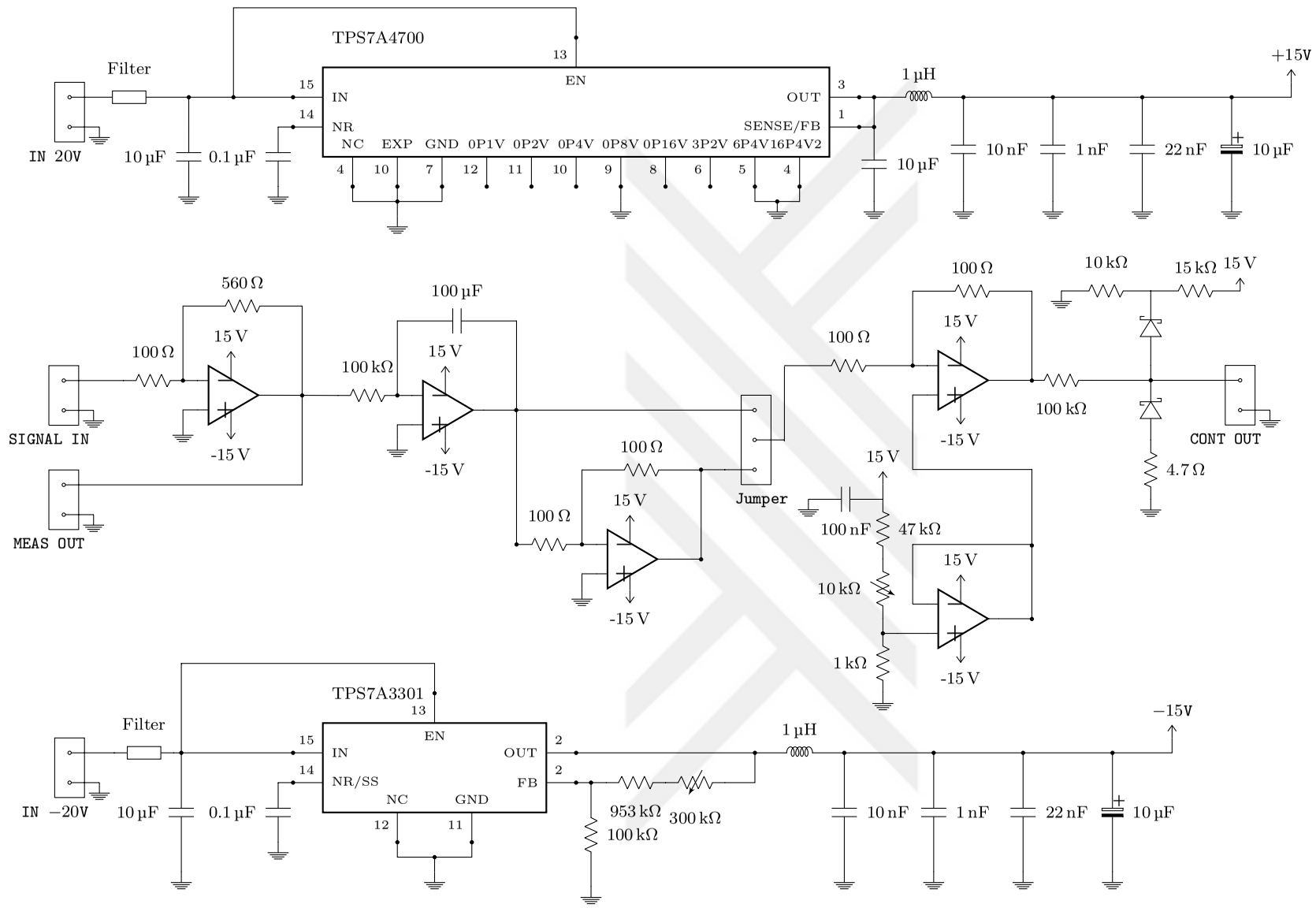

Figure 3.26: Schematics of quadrature locking circuit. All OP-AMPS are low noise OPA827. The control voltage can be inverted manually via selecting jumper position. The clipping diodes at the end ensures control voltage does not exceed phase shifter's maximum rating.

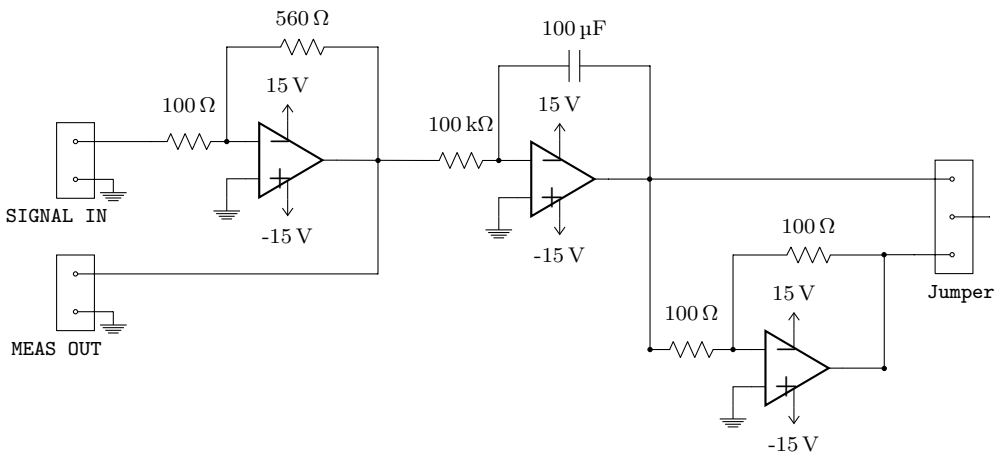

Figure 3.27: Quadrature locking circuit first stage. OP-AMPs are OPA827.

jumper position can be manually changed to invert the polarity of control signal to turn the state into negative feedback again. The `MEAS OUT` port is connected to Rohde-Schwarz Audio Analyzer for signal acquisition.

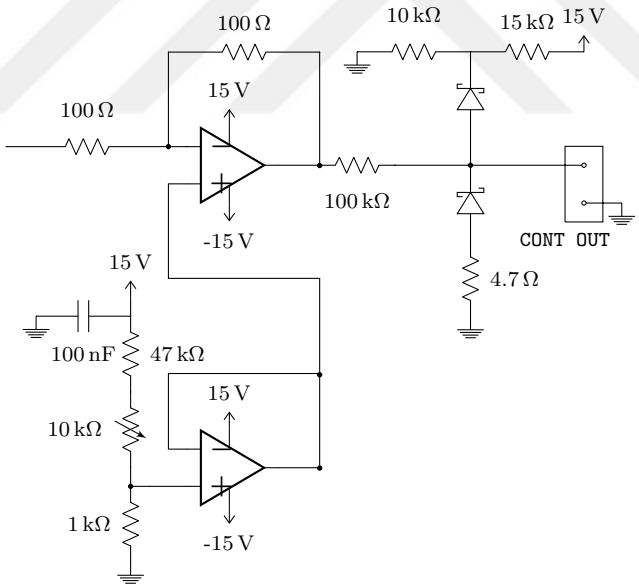

Figure 3.28: Quadrature locking circuit second stage. OP-AMPs are OPA827.

Figure 3.28 illustrates the final stage of the phase shifter control voltage. `CONT OUT` port is connected to the phase shifter's control voltage input. DC offset control with a potentiometer allows manual control of the phase shifter when the

integrator is disabled. The output is clipped to $-0.38\,\mathrm{V}$ to $6.38\,\mathrm{V}$ with Schottky diodes having a forward voltage of $0.38\,\mathrm{V}$ to protect the phase shifter when the control voltage steers to OPAMP drive voltages.

3.4 Conclusion

System operation and design principles are narrated in this section. Component specifications are provided along with the measurement methodologies of important component parameters.

The half wave voltage of the optical modulator is a key performance parameter for the system. Selecting a modulator with low half wave voltage would result in lower microwave loss in the delay line. Furthermore, with a lower half wave voltage, required RF amplifier power output to drive the modulation index closer to optimum value would be eased.

The longer delays in the frequency discriminator systems result in higher sensitivity. However, we point out that with a longer fiber, fiber optical delay line RF bandwidth is reduced due to RF power fading due to chromatic dispersion effect. Furthermore, the incident power onto the photodetector is saturated by the Stimulated Brillouin Scattering effect in the fiber. To design the fiber optical delay lines targeting higher bandwidth with longer delays, one must consider compensating such propagation effects outlined in this thesis.

Chapter 4

System Characterization and Phase Noise Measurements of Laboratory RF Synthesizers

System transfer function from the close-in phase noise of the test microwave signal to the demodulated output voltage is unknown to begin with. Baseband frequency response, system linearity and calibration constant measurements can be thoroughly carried out with a known FM tone at the input[53]. Phase noise floor of the system is assessed by removing the optical fiber from the delay line to reset sensitivity to zero and then by measuring the baseband signal at the output[32]. After the system is accurately characterized, close-in phase noise spectrum of HP8620B synthesizer, T2100 synthesizer, optoelectronic oscillator with 1 km delay and optoelectronic oscillator with 2 km are measured with our system and compared to RF spectrum analyzer E4440 measurements for verification.

4.1 System Calibration with a known FM Tone

Frequency discriminator calibration procedure described in reference [53] is adopted to our measurement system. Measuring the amplitude of the output sinusoidal signal when an FM tone with known FM frequency and modulation depth is injected to system allows end-to-end system calibration.

4.1.1 Calibration constant calculation

Calibration FM tone is generated with the help of an electronically controlled phase shifter similar to the one described in Chapter 3 Section 3.2. The system generating the FM tone is illustrated in Figure 4.1.

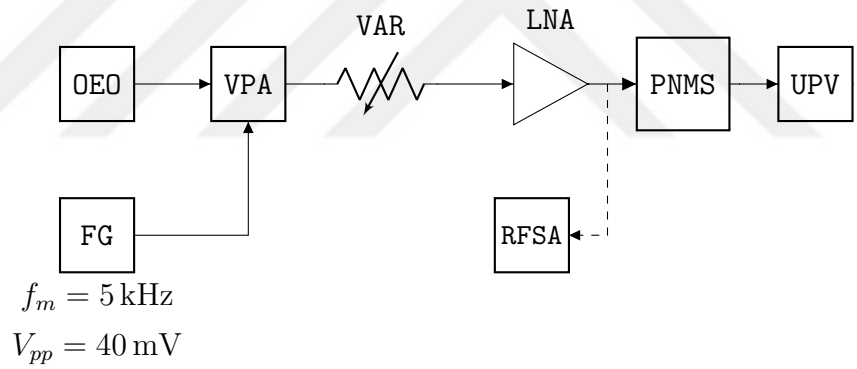

Figure 4.1: Calibration FM signal generation with an electronically controlled phase shifter. OEO: Optoelectronic oscillator with 1 km, VPA: variable phase shifter, VAR: variable attenuator, LNA: Low noise amplifier, FG: Function generator, RFSA: RF spectrum analyzer PNMS: Phase noise measurement system, UPV: Rohde-Schwarz Audio Analyzer

Optoelectronic oscillator system with 1 km and 2 km delay is provided in Figure A.1 in the appendix. Using a low phase noise source during the calibration allows calibrating with smaller FM modulation depths. Electronically controlled phase shifter modulates the phase of input microwave signal with a 5 kHz, 40 mV sinusoidal signal. Before injecting the FM signal into the phase

noise measurement system, the signal is observed on the RF spectrum analyzer to calculate modulation depth and input power. The measurement is embodied in Figure 4.2.

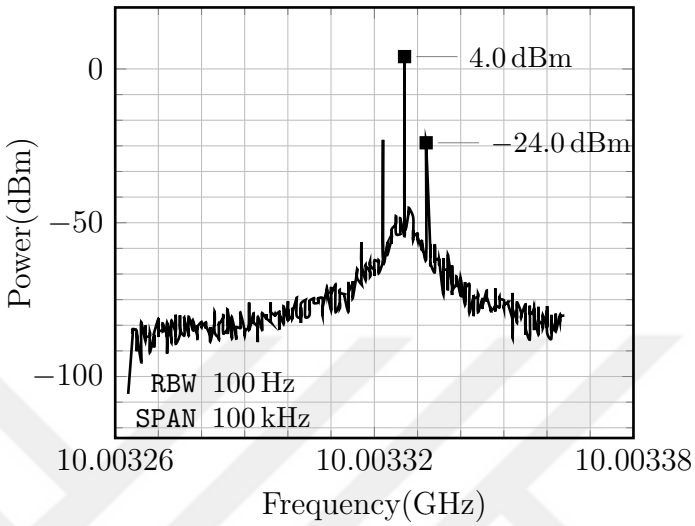

Figure 4.2: Calibration FM signal power spectrum.

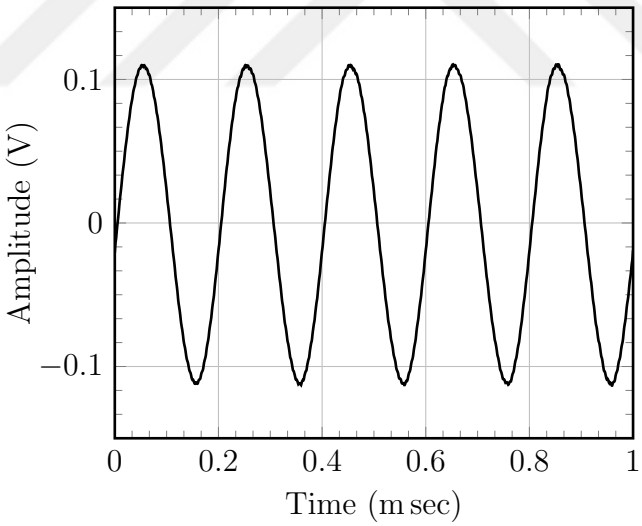

Figure 4.3: Demodulated output voltage when calibration FM is injected to system.

From Figure 4.2, the power at the fundamental frequency is set to 4.017 dBm design power. From the coupled ports of the 10 dB directional couplers at the LO and RF ports of the mixer, we record 3.4 dBm and −1.2 dBm, respectively. For

each measurement, microwave power at these taps are checked with calibrated values to ensure that the system calibration is still intact. The ratio of the fundamental microwave power to FM sideband power, $\Delta SB_{cal} = 28\,\text{dB}$. When the signal in Figure 4.2 is injected into the system, the waveform in Figure 4.3 is recorded in the `UPV` analyzer. Output waveform is a sinusoidal at 5 kHz with an rms value of $V_{rms} = 0.786\,\text{V}$.

Using the measurements for $\Delta SB_{cal} = 28\,\text{dB}$ and $V_{rms} = 0.786\,\text{V}$, calibration constant k_d is calculated as[54]

$$k_d = \frac{V_{rms}^2}{2 f_m^2 10^{\frac{\Delta SB_{cal}}{10}}} \tag{4.1}$$

$$k_d = 7.79 \cdot 10^{-8} \left[\frac{V^2}{Hz^2} \right] \tag{4.2}$$

The calibration constant in equation 4.2 is used in all the phase noise measurements presented herein. Once k_d is calculated, single sided power spectral density of the discriminator output voltage is converted to phase noise spectra of the test microwave signal with following relation[54]

$$L_f = \frac{S_v(f)}{2 f_m^2 k_d} \tag{4.3}$$

Note that equation 4.3 is not corrected for the sinc response of the calibration constant since we are not interested in offset frequencies higher than 15 kHz.

4.1.2 Frequency response and system linearity measurements

In equation 2.52, the baseband frequency response of the delay line measurement system has nulls at the frequencies equal to inverse of the delay. This property is verified by varying the FM frequency f_m in Figure 4.2 from 1 kHz to 50 kHz and recalculating the calibration constant k_d in equation 4.1 with the measured rms output voltage. The measurement is provided in Figure 4.4. For the theoretical calculation, $k_d = 7.79 \cdot 10^{-8}\ \text{V}^2/\text{Hz}^2$ as in equation 4.2 and $\tau = 25\,\mu\text{s}$ for 5 km delay.

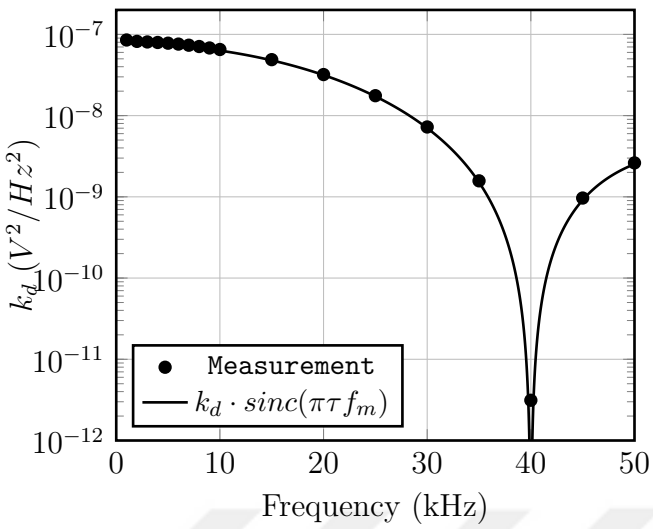

Figure 4.4: Baseband frequency response of the system.

Characteristic sinc response of the system is also observed in the measurements given in Figure 4.4.

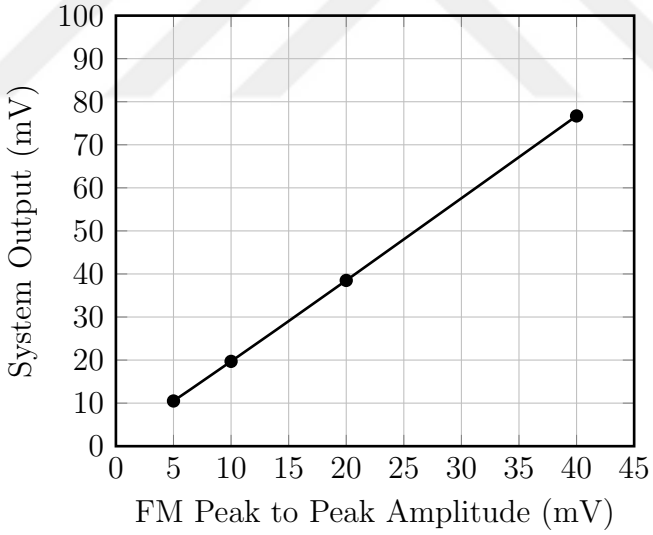

Figure 4.5: Linearity of the system.

System linearity is investigated by setting the peak to peak amplitude, V_{pp} in Figure 4.1, of FM baseband signal to 5 mV, 10 mV, 20 mV, 40 mV without changing the FM frequency. System rms output voltage is recorded for each case and embodied in Figure 4.5. Figure 4.5 indicates that system can work linearly

for sideband levels as high as -28 dBc which is much higher than the phase noise levels in practice.

4.2 Phase Noise Measurements of Laboratory RF Sources

Using the calibration results in equation 4.2, close-in phase noise spectrum of microwave synthesizers at 10 GHz can be readily measured. System phase noise floor is determined by recording measurements without fiber delay [32]. Phase noise measurements of HP83620B and T2100 synthesizers are carried out both with the spectrum analyzer E4440 and the developed system and good agreement was observed. Phase noise spectrum of optoelectronic oscillators with 1 km and 2 km delays are also depicted to demonstrate that the system can resolve close-in phase noise as low as -140 dB/Hz at 10 kHz offset from 10 GHz carrier frequency.

4.2.1 Phase Noise Floor without Delay

System sensitivity is reduced to approximately zero by removing the fiber in the delay line. Since sensitivity is close to zero, the system output when the test microwave signal is present to the input is the minimum measurable phase noise of the system [32]. Note that this method does not take into account the noise generated by the fiber itself and is somewhat optimistic[55]. For a more reliable phase noise floor measurement, an ultra low phase noise sapphire oscillators such as the one described in [56] would be the test signal to the system with the fiber delay inserted. The system output would have been the minimum measurable phase noise including the noise generated due to propagation effects in the fiber.

Time domain trace of the measured noise floor is illustrated in Figure 4.7. Trace shows 100 ms long 10 measurements stitched together. Instead of computing periodogram of the stitched signal, we averaged 10 shorter traces to have a

smoother periodogram trace. Using the MATLAB routine given in appendix, single sided power spectral density of voltage fluctuations are calculated and depicted in Figure 4.6. Conversion from voltage fluctuations to phase noise spectra is through equation 4.3 and drawn on the same plot in Figure 4.6. Minimum measurable phase noise is −147 dBc/Hz at 10 kHz offset from 10 GHz carrier frequency.

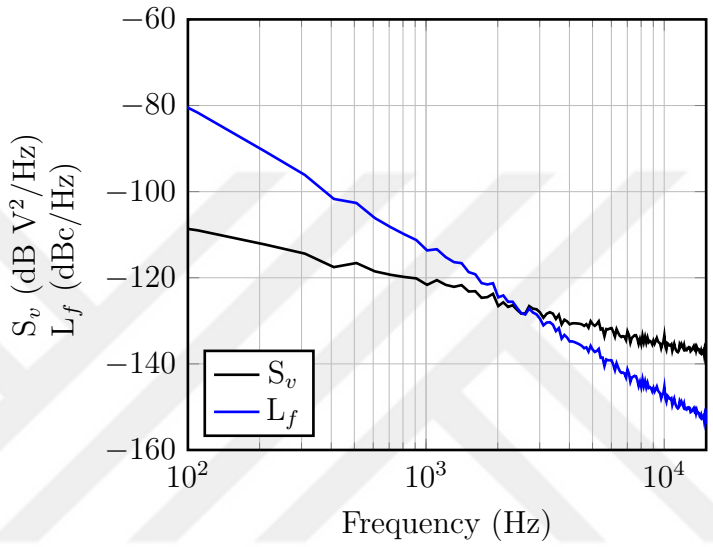

Figure 4.6: Frequency domain noise floor of the system with zero delay.

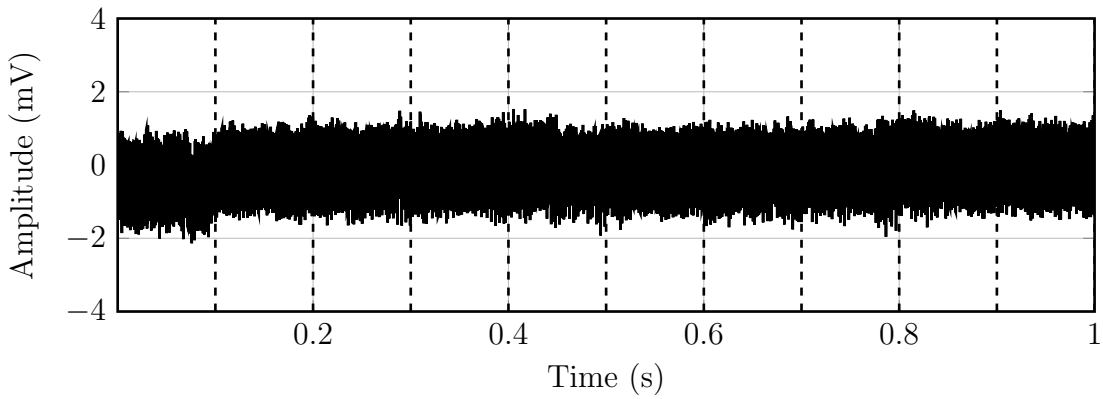

Figure 4.7: Time domain trace of system noise floor with zero delay.

4.2.2 Phase Noise Measurement Comparisons

Using the principles described above, phase noise spectrum of RF synthesizers with known phase noise is measured with the developed system and compared to the spectrum analyzer measurements.

To begin with, phase noise measurement of Hittite T2100 frequency swept synthesizer is illustrated in Figure 4.8[16]. Center frequency was set to 10 GHz and output power is 8.6 dBm. Output power is attenuated with inline RF attenuators to 4 dBm calibrated power before recording the measurement with our system.

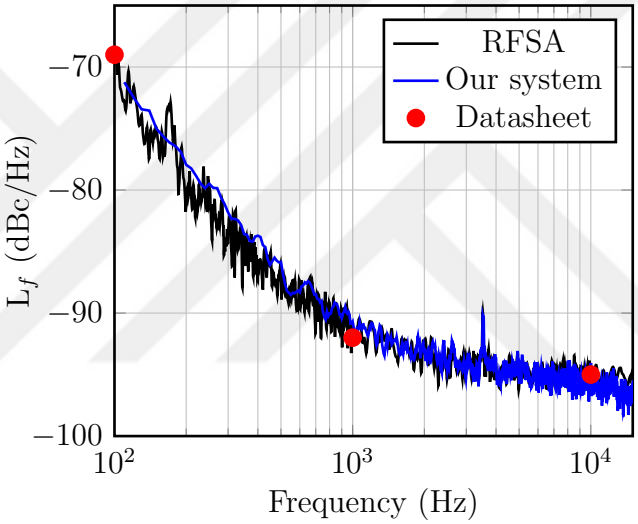

Figure 4.8: Phase noise measurement of Hittite T2100 RF synthesizer.

Datasheet values, our system's measurement and RF spectrum analyzer measurements are in excellent agreement in Figure 4.8. We also perform the same measurement with HP 83620B RF synthesizer and results are shown in Figure 4.9.

Note that the spectrum analyzer underestimates close-in phase noise of HP synthesizer since datasheet values are in good agreement with our system measurement. Phase noise measurements in Figures 4.8 and 4.9 reinforce confidence in the system measurement validity. After building trust on system validity, we measure the phase noise of optoelectronic oscillator with 1 km delay element. Detailed optoelectronic oscillator experimental set-up is embodied in Figure A.1.

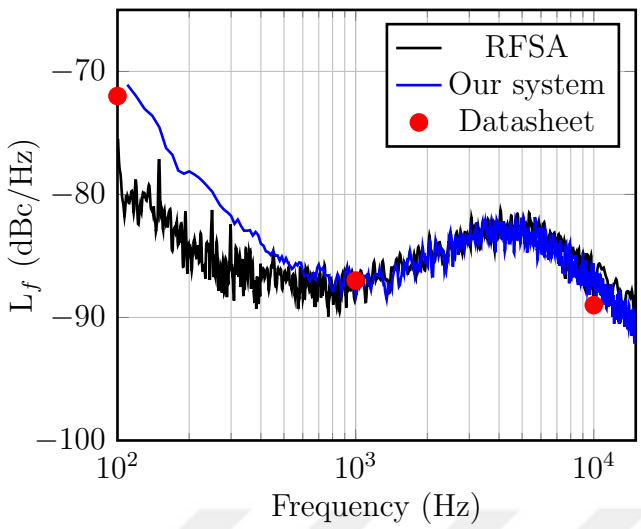

Figure 4.9: Phase noise measurement of HP 83620B RF synthesizer.

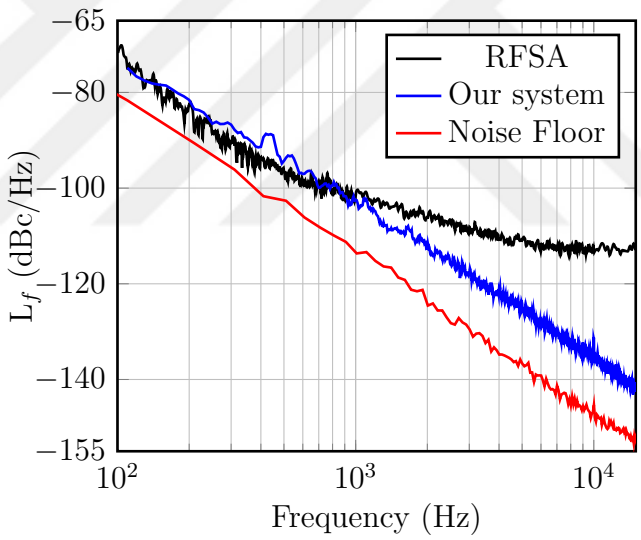

Figure 4.10: Phase noise measurement of OEO with 1 km.

Figure 4.10 shows that OEO phase noise above 1 kHz could not be resolved by the spectrum analyzer but our system can resolve such a low phase noise. For phase noise between 100 Hz and 1 kHz, good agreement is observed between the spectrum analyzer measurement and our system's measurement. The red line in Figure 4.10 indicates that OEO measurement is above system's minimum measurable phase noise.

OEO close-in phase noise reduces by the square of the delay element[7]. Hence, with 2 km OEO, phase noise would theoretically reduced by 6 dB. We measured the phase noise of the optoelectronic oscillator with 2 km delay line to test the system using this fact. Note that photocurrents must be the same in both OEO setups to observe 6 dB decrease in the phase noise. The measurement result is illustrated in Figure 4.11.

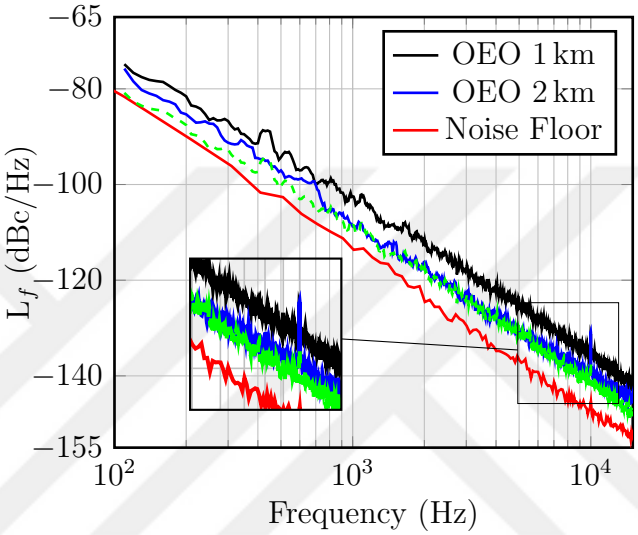

Figure 4.11: Phase noise measurement of OEO with 2 km.

The green line is calculated by subtracting 6 dB from 1 km OEO measurement. Note that the noise model for OEO described in reference [7] does not include the fiber length dependent noise described in reference [55]. For low frequencies, 2 km OEO measurements are higher than the theoretical expectation but in higher frequencies, 6 dB difference is observed. Since it is uncertain if the 2 km OEO phase noise or the system phase noise floor is the dominant noise source in low frequencies, a reference source measurement would be required to resolve the uncertainty. The noise peak at 10 kHz couples to the system from the power line; hence by considering this fact, phase noise measurement is -140 dBc/Hz at 10 kHz offset.

Chapter 5

Conclusions

Development of a delay line frequency discriminator phase noise measurement system is described in detail. Most distinguished advantage of delay line frequency discriminator method is the homodyne nature of the system not requiring a costly ultra low phase noise reference source even if the system suffers from narrow baseband frequency response due to nulls in the transfer function.

Amount of delay inserted in delayed branch of the discriminator is the most critical parameter of the system since the system sensitivity is proportional to the square of the inserted delay. Analog fiber optical delay line instead of a regular coaxial cable boosts system sensitivity by creating a delay on the order of µs which would be impractical with the coaxial cable.

Analog fiber optical delay line principally consists of a low RIN, high power laser source, a low V_π Mach-Zehnder modulator and a wide bandwidth photodetector. Half wave voltage of the modulator should be reliably measured with the described two-tone measurement method to specify microwave power budget in the system. Inherent bias drift of the modulator is stabilized with the COTS MBC-AN bias stabilizer circuit. Furthermore, effects of increasing the delay has been studied experimentally. Chromatic dispersion and stimulated Brillouin scattering have deleterious impacts on the system microwave bandwidth and allowable

injected power into the fiber. Additional measures are described which have to be taken to circumvent the negative effects of longer fiber. Longer delay also limits the baseband bandwidth of the measurement system. Selection of 5 km fiber generating 25 µs delay served our purpose to resolve the phase noise at 10 GHz carrier and 10 kHz offset frequency.

Length of the fiber together with the center frequency of the test signal fluctuates in time making it difficult to maintain quadrature condition on mixer. An OPAMP integrator locking circuit is designed to automatically stabilize the mean of the output signal at zero.

The polarity of phase difference between RF and LO ports of the mixer may require manual switching of the integrator circuit to prevent positive feedback in the circuit. An automatic threshold detection circuit with a transistor switch would allow fully automated measurement. Furthermore, an internal synthesizer with FM capability would also allow automatic and periodic calibration and could be considered as a future feature.

Bibliography

[1] J. Yao, "Microwave photonics," *Journal of Lightwave Technology*, vol. 27, pp. 314–335, Feb 2009.

[2] J. C. N. Dalma, "Microwave photonics combines two worlds," *Nature Photonics*, vol. 1, pp. 319–330, Jun 2007.

[3] R. Benjamin and A. J. Seeds, "Optical beam forming techniques for phased array antennas," *IEE Proceedings H - Microwaves, Antennas and Propagation*, vol. 139, pp. 526–534, Dec 1992.

[4] J. Capmany, B. Ortega, and D. Pastor, "A tutorial on microwave photonic filters," *Journal of Lightwave Technology*, vol. 24, pp. 201–229, Jan 2006.

[5] M. Y. Frankel, J. U. Kang, and R. D. Esman, "High-performance photonic analogue-digital converter," *Electronics Letters*, vol. 33, pp. 2096–2097, Dec 1997.

[6] J. D. McKinney, D. S. Seo, and A. M. Weiner, "Photonically assisted generation of continuous arbitrary millimetre electromagnetic waveforms," *Electronics Letters*, vol. 39, pp. 309–311, Feb 2003.

[7] X. S. Yao and L. Maleki, "Optoelectronic oscillator for photonic systems," *IEEE Journal of Quantum Electronics*, vol. 32, pp. 1141–1149, July 1996.

[8] E. Rubiola, E. Salik, S. Huang, N. Yu, and L. Maleki, "Photonic-delay technique for phase-noise measurement of microwave oscillators," *J. Opt. Soc. Am. B*, vol. 22, pp. 987–997, May 2005.

[9] J. F. Diehl, J. M. Singley, C. E. Sunderman, and V. J. Urick, "Microwave photonic delay line signal processing," *Appl. Opt.*, vol. 54, pp. F35–F41, Nov 2015.

[10] L. M. X.S. Yao, "Influence of an externally modulated photonic link on a microwave communications system," tech. rep., NASA, 1994.

[11] D. Eliyahu, D. Seidel, and L. Maleki, "Rf amplitude and phase-noise reduction of an optical link and an opto-electronic oscillator," *IEEE Transactions on Microwave Theory and Techniques*, vol. 56, pp. 449–456, Feb 2008.

[12] P. Salzenstein, J. Cussey, X. Jouvenceau, H. Tavernier, L. Larger, E. Rubiola, and G. Sauvage, "Realization of a phase noise measurement bench using cross correlation and double optical delay line," *Acta Physica Polonica A*, vol. 112, pp. 1107–1111, 11 2007.

[13] "IEEE standard definitions of physical quantities for fundamental frequency and time metrology—random instabilities," *IEEE Std Std 1139-2008*, pp. c1–35, Feb 2009.

[14] E. Rubiola, *Phase Noise and Frequency Stability in Oscillators (The Cambridge RF and Microwave Engineering Series)*. Cambridge University Press, 2009.

[15] J. Rutman, "Characterization of phase and frequency instabilities in precision frequency sources: Fifteen years of progress," *Proceedings of the IEEE*, vol. 66, pp. 1048–1075, Sept 1978.

[16] "HMC-T2100 synthesized signal generator, 10 mhz to 20 ghz." `http://http://www.analog.com/media/en/technical-documentation/data-sheets/hmc-t2100.pdf`. Accessed: 2018-10-7.

[17] E. Rubiola, "Basics of phase noise." IEEE Frequency Control Symposium (FCS) and PTTI Joint Conference, Vancouver, Canada, August 2005.

[18] J. J. Grobbelaar, "Phase noise measurement techniques," Master's thesis, Stellenbosch University, March 2011.

[19] C. Group, *Frequency Measurement and Control*, ch. 4, p. 105. No. 9781461360650 in Microwave Technology Series, Chapman and Hall, 1994.

[20] "Application note 150: Spectrum analyzer basics." `http://literature.cdn.keysight.com/litweb/pdf/5952-0292.pdf`. Accessed: 2018-11-1.

[21] "Application note 150: Spectrum analyzer basics." `http://literature.cdn.keysight.com/litweb/pdf/5952-0292.pdf`. Accessed: 2018-11-1.

[22] *Agilent Technologies PSA Series Spectrum Analyzers Specifications Guide*, ch. 2, p. 117. Agilent, 2012.

[23] "Product note 11729c-2: Phase noise characterization of microwave oscillator: Frequency discriminator method." `http://www.thegleam.com/ke5fx/gpib/11729c2.pdf`. Accessed: 2018-11-1.

[24] D. Middleton, *Statistical Communication Theory*, ch. 14, p. 601. IEEE Press.

[25] O. K. Okusaga, "Photonic delay-line phase noise measurement system," tech. rep., US Army Research Laboratory, 2011.

[26] P. Brochard, T. Südmeyer, and S. Schilt, "Power spectrum computation for an arbitrary phase noise using middleton's convolution series: Implementation guideline and experimental illustration," *IEEE Transactions on Ultrasonics, Ferroelectrics, and Frequency Control*, vol. 64, pp. 1766–1775, Nov 2017.

[27] "Product note 11729c-2: Phase noise characterization of microwave oscillator: Phase detector method." `https://www.keysight.com/upload/cmc_upload/All/5952-8286E.pdf`. Accessed: 2018-11-2.

[28] C. Group, *Frequency Measurement and Control*, ch. 2, pp. 51–52. No. 9781461360650 in Microwave Technology Series, Chapman and Hall, 1994.

[29] "The magic of cross correlation in measurements from dc to optics." `http://www.rubiola.org/pdf-articles/conference/2008-eftf-magic-correlation.pdf`. Accessed: 2018-11-2.

[30] "Agilent 8360b series synthesized swept signal generators datasheet." https://literature.cdn.keysight.com/litweb/pdf/5964-6162E.pdf?id=1000030846:epsg:dow. Accessed: 2018-10-7.

[31] E. Rubiola, "Tutorial on the double balanced mixer." https://arxiv.org/pdf/physics/0608211.pdf. Accessed: 2018-10-7.

[32] K. Volyanskiy, J. Cussey, H. Tavernier, P. Salzenstein, G. Sauvage, L. Larger, and E. Rubiola, "Applications of the optical fiber to the generation and measurement of low-phase-noise microwave signals," *J. Opt. Soc. Am. B*, vol. 25, pp. 2140–2150, Dec 2008.

[33] D. M. K. J. W. Vincent J. Urick, Jr. Jason, *Fundamentals of Microwave Photonics*, ch. 6, p. 215. Wiley, 2015.

[34] M. B.E.A. Saleh, *Fundamentals of Photonics*, ch. 9, p. 340. Wiley, 2 ed., 2007.

[35] Cisco, "Cisco ons 15454 dwdm engineering and planning guide, release 7.x." https://www.cisco.com/c/en/us/td/docs/optical/15000r7_0/dwdm/planning/guide/70epg/d7ovw.html. Accessed: 2018-11-7.

[36] "Analog mz modulator bias controller." https://photonics.ixblue.com/store/modulator-matching-components/analog-mz-modulator-bias-controller. Accessed: 2019-01-05.

[37] O. K. Okusaga, "Photonic delay-line phase noise measurement system," tech. rep., US Army Research Laboratory, 2011.

[38] "R-s-upv audio analyzer." https://www.rohde-schwarz.com/us/product/upv-productstartpage_63493-7558.html. Accessed: 2019-01-05.

[39] K. J. W. Vincent J. Urick Jr., Jason . McKinney, *Fundamentals of Microwave Photonics*, ch. 6, pp. 212–213. John Wiley & Sons, Inc, 2015.

[40] X. S. Yao and L. Maleki, "Optoelectronic oscillator for photonic systems," *IEEE Journal of Quantum Electronics*, vol. 32, pp. 1141–1149, July 1996.

[41] K. J. W. Vincent J. Urick Jr., Jason . McKinney, *Fundamentals of Microwave Photonics*, ch. 1, pp. 20–21. John Wiley & Sons, Inc, 2015.

[42] K. J. W. Vincent J. Urick Jr., Jason . McKinney, *Fundamentals of Microwave Photonics*, ch. 6, p. 221. John Wiley & Sons, Inc, 2015.

[43] G. K. Gopalakrishnan, W. K. Burns, R. W. McElhanon, C. H. Bulmer, and A. S. Greenblatt, "Performance and modeling of broadband linbo/sub 3/ traveling wave optical intensity modulators," *Journal of Lightwave Technology*, vol. 12, pp. 1807–1819, Oct 1994.

[44] Y. Di, P. Gardner, and H. Ghafouri-Shiraz, "Methods for measuring the rf half-wave voltage of linbo3 optical modulators," *Microwave and Optical Technology Letters*, vol. 46, no. 5, pp. 440–443.

[45] E. Blanchard, "Optical fiber." `http://epq.com.co/softw_internet/nag1/x1077.htm`. Accessed: 2018-11-7.

[46] K. J. W. Vincent J. Urick Jr., Jason . McKinney, *Fundamentals of Microwave Photonics*, ch. 5, pp. 177–178. John Wiley & Sons, Inc, 2015.

[47] G. E. Agrawal, *Fiber-Optic Communication Systems*, ch. 7, p. 288. John Wiley & Sons, Inc, 2002.

[48] G. Agrawal, "Chapter 9 - stimulated brillouin scattering," in *Nonlinear Fiber Optics (Fifth Edition)* (G. Agrawal, ed.), Optics and Photonics, pp. 353 – 396, Boston: Academic Press, fifth edition ed., 2013.

[49] A. B. Ruffin, "Stimulated brillouin scattering: an overview of measurements, system impairments, and applications," in *Technical Digest: Symposium on Optical Fiber Measurements, 2004.*, pp. 23–28, Sep. 2004.

[50] G. Agrawal, *Chapter 9 - Stimulated Brillouin Scattering*, ch. 9, p. 339. John Wiley & Sons, Inc, 2013.

[51] D. Eliyahu and L. Maleki, "Low phase noise and spurious level in multi-loop opto-electronic oscillators," in *IEEE International Frequency Control Symposium and PDA Exhibition Jointly with the 17th European Frequency and Time Forum, 2003. Proceedings of the 2003*, pp. 405–410, May 2003.

[52] K. Volyanskiy, *The study of phase noise spectra of a microwave delay line optoelectronic oscillator*. PhD thesis, Université de Franche-Comté, 2009.

[53] "Phase noise characterization of microwave oscillator frequency discriminator method product note 11729c-2." `http://www.thegleam.com/ke5fx/gpib/5952-8286e.pdf`. Accessed: 2019-01-19.

[54] "Product note 11729c-2: Phase noise characterization of microwave oscillator: Frequency discriminator method." `http://www.thegleam.com/ke5fx/gpib/11729c2.pdf`. Accessed: 2018-11-1.

[55] A. Docherty, C. R. Menyuk, O. Okusaga, and W. Zhou, "Stimulated rayleigh scattering and amplitude-to-phase conversion as a source of length-dependent phase noise in oeos," in *2012 IEEE International Frequency Control Symposium Proceedings*, pp. 1–5, May 2012.

[56] "The leeson effect: Phase noise and frequency stability in oscillators." `http://rubiola.org/pdf-slides/2011T-IFCS-Leeson-effect.pdf`. Accessed: 2018-11-1.

Appendix A

Single loop optoelectronic oscillator

Optoelectronic oscillators are emerging RF frequency synthesizers capable of producing very high spectral purity microwave/millimeter wave signals[7]. System is basically a delay line oscillator with many resonator modes separated by the inverse of the delay. For example, for 1 km fiber, frequency separation is 200 kHz and for 2 km fiber it is 100 kHz vice versa. As the delay increases, similar to a Fabry-Perot interferometer, resonator peaks becomes sharper and denser. The oscillating mode is selected with a high Q bandpass filter. With a 16 km delay element and a bandpass filter with 38000 Q, phase noise of −165 dBc/Hz at 10 kHz offset from 10 GHz center frequency is achieved[11]. Figure A.1 illustrates complete set-up of optoelectronic oscillator Rf synthesizers developed to test the measurement system. When the delay element is changed, optical power incident onto the photodetector is adjusted to 55 µW at the tap and RF power output from the oscillator is adjusted with variable attenuator in the loop and is coupled with a 10 dB RF coupler.

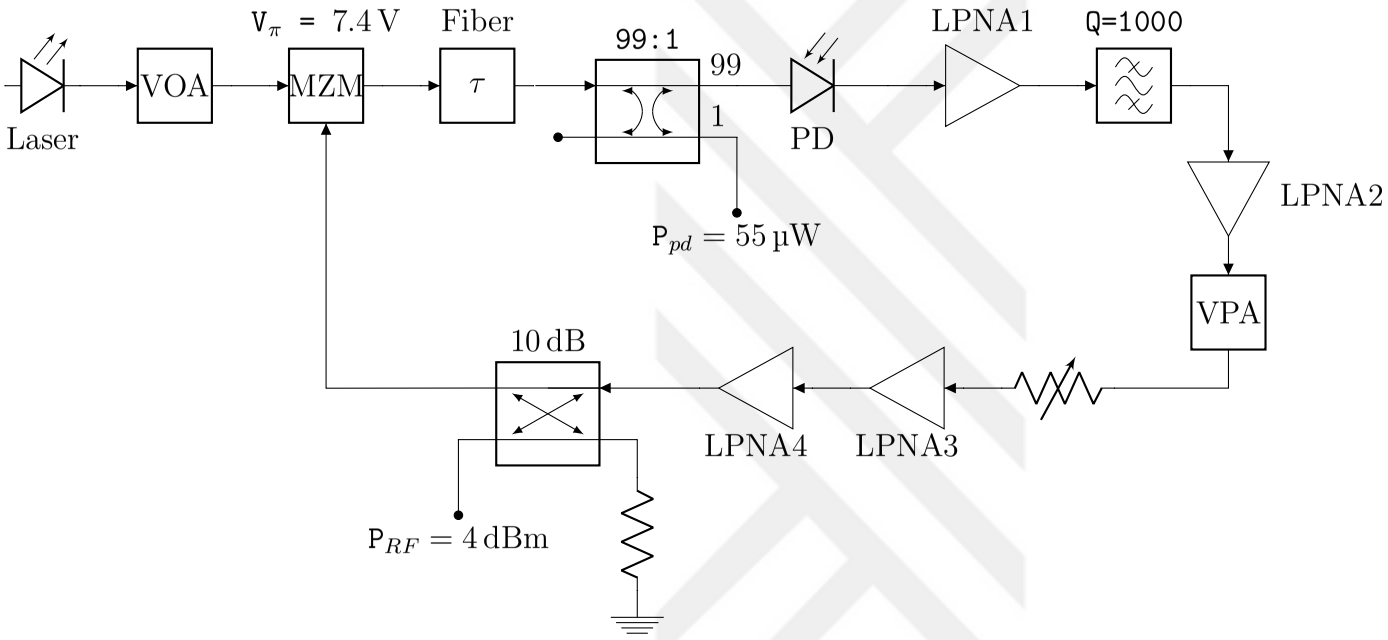

Figure A.1: Block diagram of optoelectronic oscillator[7]. LPN: Low Phase Noise Amplifier, 10dB: 10dB directional coupler, VPA: Variable phase shifter, PD: photodetector, MZM: Mach-Zehnder Intensity Modulator,Fiber: 1 km and 2 km single mode fiber cable, mode selection in the resonator is accomplished by the bandpass filter with a Q of 1000.

Appendix B

Matlab scripts

Following MATLAB subroutines are utilized to compute phase noise spectra from time domain voltage recordings.

```
    function [f, S_f1] = computePSD(data, T, numOfAverages, fs)
    %% Compute One Sided Power Spectral Density of input time ...
        signal in V^2/Hz
    % T: miliseconds
    % data: time domain voltage in volts
    % fs: sampling frequency in fs
    blck = fs*T*1e-3;
    pxx1 = 0;
    for i = 1:numOfAverages
        strt_i = blck*(i-1)+1;
        stp_i = blck*i;
        d1 = data(strt_i:stp_i,1);
        [pxx_1,f] = periodogram(d1,[],length(d1),fs,'psd');
        pxx1 = pxx1 + pxx_1;
        disp(['Completed ', num2str(i), 'th of ', ...
            num2str((numOfAverages))]);
    end

pxx1 = pxx1/numOfAverages;
f = f(2:end); % don't plot DC
```

```
S_f1 = pxx1(2:end);
end
```

```
    % close all
    % clear
    % clc
    %% Photonic-delay technique for phase-noise measurement ...
        of microwave oscillators
    %% Load Data
    inDat = load('floor.mat');
    fs = 768e3;
    [freq_axis, S_v] = computePSD(inDat.data, 100, 10, fs); % ...
        in V^2/Hz
    %% Calibration Parameters
    tau = 25e-6;
    Kfac = 7.79e-8;
    Sphi = S_v./((freq_axis.^2)*Kfac);
    Sphi = 10*log10(smooth(Sphi)) - 3;
    %% Plot
    %f1 = figure(1);
    %semilogx(downsample(freq_axis,1),downsample(Sphi,1));
    %grid on
    %hold on
```